The Analysis of General Axially Symmetric Antennas with a Coaxial Feed Line by the Method of Lines

Reinhold Pregla, *Senior Member, IEEE*

***Abstract*— The use of the method of lines in the analysis of various circular antennas—circular patch antennas and various forms of monopoles is proposed and substantiated. The antennas considered are fed by coaxial lines. Impedance/admittance transfer procedures are developed, which allow to calculate the antenna input impedance by a successive transfer from the aperture through the different sections. The described relations are also useful for other applications.**

***Index Terms*— Antennas, crossed discretization lines, dipoles, impedance/admittance transfer concept, method of lines, microstrip antennas, planar antennas.**

I. Introduction

THE increasing importance of planar and different types of monopole antennas in microwave engineering calls for exact models for their simulation. Planar antennas are constructed by a metallized (ground side) substrate with metallic patches on the back side. The patches are fed either by striplines on the side of the patches, or by coaxial lines from the ground side. Generally, the patches may have rectangular, circular, or any other forms. The forms of monopoles are dependent on applications and are complex in some cases.

In this paper, the method of lines (MoL), a special finite-difference method, is proposed for analysis of general forms of circular antennas—especially circular patch antennas and different forms of monopoles (Fig. 1) with coaxial feed line. It has been shown in a large number of papers that the MoL is highly suitable for analysis of electromagnetic field problems [1]–[13] in single- or multilayered planar and cylindrical structures, using discretization of the relevant partial differential equations in various coordinate systems. In the MoL, the field is discretized only as long as necessary. In this case, the discretization is as follows. In the coaxial feeding line the field will be discretized in radial direction. Therefore, the discretization lines on which the field is described analytically, have longitudinal direction. In the substrate, in the radial line, above the patch and the monopole and in the outer region, the discretization is carried out in vertical direction (Fig. 2). In radial direction the field is described analytically by cylinder functions. In the transition region from the coaxial line to the parallel-plate radial waveguide the field is decomposed into two parts. These parts can be treated as a continuation of the fields in the coaxial line and parallel-plate radial waveguide, respectively. Therefore, these parts are also discretized on the continuation of the discretization lines of neighboring regions which cross each other. In this way, the wave transition from the vertical (coaxial line) to the radial direction can be described very easily.

An impedance/admittance transfer procedure is given for all of the regions which allows to calculate the input impedance in the coaxial line by a successive numerically stable transfer from the aperture through the different sections of the structure considered. The number of sections is not limited. Therefore, very complex structures can be analyzed. Then the field in the whole structure can be calculated by introducing a source wave

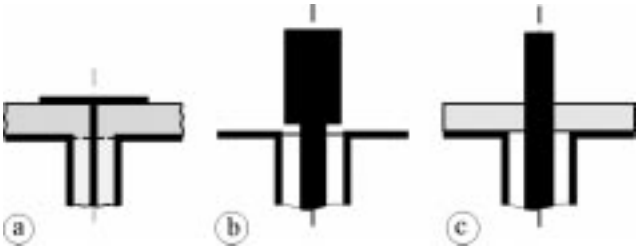

Fig. 1. Circular patch antenna and two types of monopole antennas.

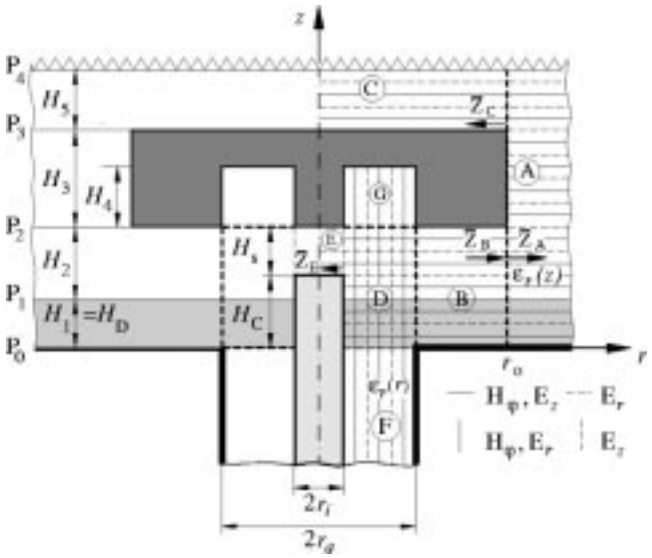

Fig. 2. General structure of a circular planar antenna.

Manuscript received September 29, 1997; revised June 2, 1998.

The author is with Allgemeine und Theoretische Elektrotechnik, Fern Universität, Hagen, D-58084 Germany.

Publisher Item Identifier S 0018-926X(98)07490-0.

in the coaxial line. As usual in transmission line theory, the field is calculated in reversel direction; that means in direction from source to load (aperture). This is completely analogous to [10]. To simulate an open structure at a suitable distance above the patch, absorbing boundary conditions (ABC) are introduced. Results are presented for the input impedance and field distribution.

II. Theory

The general structure to be considered is sketched in Fig. 2. In this general structure all the antenna forms in Fig. 1 are included. If the planes P_1 and P_2 are moved together so that they coincide, the structure reduces to a normal patch antenna. The patch may be either of finite thickness or infinitely thin. If H_3 in Fig. 2 is increased to the order of a quarter wavelength, the normal coaxial fed monopole [Fig. 1(b)] is obtained. In case of the monopole shown in Fig. 1(c), the plane P_2 is replaced by ABC's. In the general case, ABC's are introduced in plane P_4. Because the efficiency of ABC's in dependent on the angle of incidence [2] they must be chosen carefully. If we assume that the radiation into region C and toward ABC's takes place from the upper metallic edge then the height H_5 should be greater than r_0. This is because we can achieve high enough absorption for incidence angles up to 45°. In region A, the reflected radiation field at the ABC's does not come back to the antenna. Therefore, in this region the problem is not so sensitive.

The partitioning of the structure in subregions must be done in such a way that in each of the subregions the field can be described completely after the discretization. Nevertheless there is some degree of freedom. For example, the combination of the regions B and D with crossed-line systems can be used instead of two separate regions. But as it will be seen later the field impedance (admittance), transfer from one region to another is very simple and highly accurate. Hence, it is better to use more subregions than less. In this way there is also the possibility to divide the region A in, e.g., three subregions: two as continuations of subregions B and C, respectively, with crossed line systems. The third is the region between these two with discretization lines in vertical direction. The vertical discretization lines must have a last one at $r_1 > r_0$ with ABC's. In this paper, we would not make use of this possibility. But it will again improve the accuracy. A cylindrical coordinate system (r, φ, z) with z axis along the inner conductor of the coaxial line is the obvious one to use in the analysis so that the boundaries of the structure are described simply by parts of coordinate surfaces.

A. Basic Equations

In this subsection, the fundamental equations for the above mentioned general structure are derived. The structure is completely circularly symmetric. The TEM field of the coaxial feed line is also independent of the azimuthal angle φ, so we have $\partial/\partial\varphi = 0$. The only nonzero components are H_φ, E_r, and E_z. The permittivity ε_r is assumed to be a function of r or z: $\varepsilon_r = \varepsilon_r(r)$ or $\varepsilon_r = \varepsilon_r(z)$. The wave equation is directly obtained from Maxwell's equations.

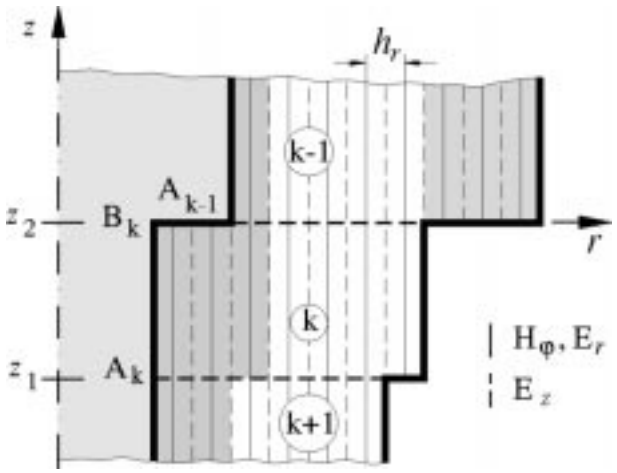

Fig. 3. Concatenations of the coaxial waveguide sections. The permittivities are functions of r.

From the general vectorial wave equation

$$\nabla \times \left(\frac{1}{\varepsilon_r} \nabla \times \vec{H} \right) - k_0^2 \vec{H} = 0 \tag{1}$$

the reduced form of the scalar wave equation for the azimuthal field component $\tilde{H}_\varphi$ is obtained

$$\varepsilon_r \frac{\partial}{\partial \overline{r}} \left(\frac{1}{\varepsilon_r \overline{r}} \frac{\partial}{\partial \overline{r}} (\overline{r} \tilde{H}_\varphi) \right) + \varepsilon_r \frac{\partial}{\partial \overline{z}} \left(\varepsilon_r^{-1} \frac{\partial \tilde{H}_\varphi}{\partial \overline{z}} \right) + \varepsilon_r \tilde{H}_\varphi = 0 \tag{2}$$

where the following normalizations are introduced: $\tilde{H}_\varphi = \eta_0 H_\varphi$, $\overline{r} = k_0 r$, $\overline{z} = k_0 z$, η_0, and k_0 being the wave impedance and wave number of free-space, respectively.

The electric field components are given by

$$j\varepsilon_r E_r = -\frac{\partial \tilde{H}_\varphi}{\partial \overline{z}} \qquad j\varepsilon_r E_z = \frac{1}{\overline{r}} \frac{\partial}{\partial \overline{r}} (\overline{r} \tilde{H}_\varphi). \tag{3}$$

B. Discretization, Transformation, and General Solutions

The direction of discretization depends on the region of the structure (Fig. 2). In the region of the coaxial line (F, G) the discretization in radial coordinate direction has to be performed, whereas in the planar regions (A, B, C, and E) the discretization is in z direction. In transition region D (coaxial line—parallel plate radial waveguide) crossed discretization line systems are used.

1) Coaxial Line Sections: In general, the coaxial line part consists of concatenations of sections with different radii (see Fig. 3). The solution for the fields in each of these sections is obtained by discretizing the equations in radial direction r. The discretization lines are shown in Fig. 2 and in detail in Fig. 3. The discretization line numeration follows the positive r direction. The permittivity can be a function of r. Variations in z direction should be modeled by as many as necessary sections. For an arbitrary kth section the discretization yields

$$\tilde{H}_\varphi \rightarrow \tilde{\mathbf{H}}_\varphi \tag{4}$$

$$E_r \rightarrow \mathbf{E}_r \tag{5}$$

$$\overline{r} \rightarrow \boldsymbol{r}_h, \boldsymbol{r}_e \tag{6}$$

$$\varepsilon \rightarrow \boldsymbol{\epsilon}_h, \boldsymbol{\epsilon}_e \tag{7}$$

$$\frac{\partial}{\partial \overline{r}} \rightarrow \overline{h}_r^{-1} \boldsymbol{D}_r = \overline{\boldsymbol{D}}_r. \tag{8}$$

The components in the vector $\tilde{\mathbf{H}}_\varphi$ ($\mathbf{E}_r$) are the values of $\tilde{H}_\varphi$ (E_r) on all of the full discretization lines. The discretized radii (permittivities) of these lines are collected in the diagonal matrix $\boldsymbol{r}_h$ ($\boldsymbol{\epsilon}_h$). The discretized radii (permittivities) on the dashed lines are collected in the diagonal matrix $\boldsymbol{r}_e$ ($\boldsymbol{\epsilon}_e$). The discretized values of E_z are given also on these lines. The difference operator matrix $\boldsymbol{D}_r$ has to fulfill the Neumann boundary conditions. All the discretized quantities should be marked with a sub- or superscript for the section under consideration, which we mostly omit for the sake of brevity.

Since the difference operator matrices are not diagonal, we must perform a transformation to the principal axes yielding the following:

$$\tilde{\mathbf{H}}_\varphi = \boldsymbol{T}_r \overline{\mathbf{H}}_\varphi \quad \boldsymbol{T}_r^{-1}(\boldsymbol{\epsilon}_h \overline{\boldsymbol{D}}_r^t \boldsymbol{\epsilon}_e^{-1} \boldsymbol{r}_e^{-1} \overline{\boldsymbol{D}}_r \boldsymbol{r}_h - \boldsymbol{\epsilon}_h) \boldsymbol{T}_r = \boldsymbol{\Gamma}_z^2. \tag{9}$$

The superscript t denotes the transpose matrix, $\boldsymbol{\Gamma}_z^2$ is diagonal matrix of eigenvalues, and transformation matrix $\boldsymbol{T}_r$ contains the eigenvectors of the term in parenthesis. The discretized and transformed wave equation and its general solution are given by

$$\frac{d^2 \overline{\mathbf{H}}_\varphi}{d\overline{z}^2} - \boldsymbol{\Gamma}_z^2 \overline{\mathbf{H}}_\varphi = \mathbf{0} \qquad \overline{\mathbf{H}}_\varphi = e^{-\boldsymbol{\Gamma}_z \overline{z}} \mathbf{A} + e^{\boldsymbol{\Gamma}_z \overline{z}} \mathbf{B}. \tag{10}$$

For the radial electric field component we obtain

$$\overline{\mathbf{E}}_r = -j \boldsymbol{\epsilon}_h^{-1} \boldsymbol{\Gamma} (e^{-\boldsymbol{\Gamma} \overline{z}} \mathbf{A} - e^{\boldsymbol{\Gamma} \overline{z}} \mathbf{B}). \tag{11}$$

From the parts of electric and magnetic vector describing the propagation in $+z$ direction (i.e., in forward direction—subscript f), we define a characteristic wave impedance/admittance matrix (normalized by to the free-space wave impedance η_0) by

$$\overline{\mathbf{E}}_{rf} = \overline{\mathbf{Z}}_{0z} \overline{\mathbf{H}}_{\varphi f} \qquad \overline{\mathbf{H}}_{\varphi f} = \overline{\boldsymbol{Y}}_{0z} \overline{\mathbf{E}}_{rf} \tag{12}$$

$$\overline{\boldsymbol{Z}}_{0z} = -j \boldsymbol{\epsilon}_h^{-1} \boldsymbol{\Gamma}_z \qquad \overline{\boldsymbol{Y}}_{0z} = \overline{\boldsymbol{Z}}_{0z}^{-1}. \tag{13}$$

For the fundamental mode (ith propagating mode) the corresponding propagation constant $\boldsymbol{\Gamma}_{zi}$ is purely imaginary and the related $\boldsymbol{Z}_{0i}$ becomes real. Now the relation between the fields at the boundaries A ($z = z_1$) and B ($z = z_2$) of a section (e.g., k in Fig. 3) can be written as generalized transmission line equations

$$\begin{bmatrix} \overline{\mathbf{E}}_{r\mathrm{A}} \\ \overline{\mathbf{E}}_{r\mathrm{B}} \end{bmatrix} = \begin{bmatrix} \overline{\mathbf{z}}_1 & \overline{\mathbf{z}}_2 \\ \overline{\mathbf{z}}_2 & \overline{\mathbf{z}}_1 \end{bmatrix} \begin{bmatrix} \overline{\mathbf{H}}_{\varphi\mathrm{A}} \\ -\overline{\mathbf{H}}_{\varphi\mathrm{B}} \end{bmatrix} \tag{14}$$

with

$$\overline{\mathbf{z}}_1 = \overline{\boldsymbol{Z}}_{0z} (\tanh(\boldsymbol{\Gamma}_z \overline{d}))^{-1} \qquad \overline{\mathbf{z}}_2 = \overline{\boldsymbol{Z}}_{0z} (\sinh(\boldsymbol{\Gamma}_z \overline{d}))^{-1} \tag{15}$$

where $\overline{d} = k_0(z_2 - z_1)$ is the length of this section normalized with k_0. The negative sign at $\overline{\mathbf{H}}_{\varphi\mathrm{B}}$ is introduced similar as in the network theory using scalar z parameters for describing voltage–current port relations. Defining the impedance matrices $\overline{\mathbf{Z}}_{\mathrm{A,B}}$ in the cross sections A and B by

$$\overline{\mathbf{E}}_{r\mathrm{A,B}} = \overline{\mathbf{Z}}_{\mathrm{A,B}} \overline{\mathbf{H}}_{\varphi\mathrm{A,B}} \tag{16}$$

the impedance transfer in a section yields for both directions

$$\overline{\boldsymbol{Z}}_{\mathrm{A}} = \overline{\mathbf{z}}_1 - \overline{\mathbf{z}}_2 (\overline{\mathbf{z}}_1 + \overline{\boldsymbol{Z}}_{\mathrm{B}})^{-1} \overline{\mathbf{z}}_2 \tag{17}$$

$$-\overline{\mathbf{Z}}_{\mathrm{B}} = \overline{\mathbf{z}}_1 - \overline{\mathbf{z}}_2 (\overline{\mathbf{z}}_1 + (-\overline{\boldsymbol{Z}}_{\mathrm{A}}))^{-1} \overline{\mathbf{z}}_2. \tag{18}$$

The impedances $-\overline{\boldsymbol{Z}}_{\mathrm{A}}$ and $-\overline{\boldsymbol{Z}}_{\mathrm{B}}$ are the impedances for looking in $-z$ direction. Instead of (18) we may also use the inverted relation with the matrix parameters

$$\overline{\boldsymbol{y}}_1 = \overline{\boldsymbol{Y}}_{0z} (\tanh(\boldsymbol{\Gamma}_z \overline{d}))^{-1} \qquad \overline{\boldsymbol{y}}_2 = -\overline{\boldsymbol{Y}}_{0z} (\sinh(\boldsymbol{\Gamma}_z \overline{d}))^{-1}. \tag{19}$$

The admittance transfer along a section is completely analogous to the impedance transfer. The impedance/admittance transfer between the two sides of the common plane of two adjacent sections can be performed by the general formula derived in [10] or in specific form in [11] even in case of offsets (Fig. 3) and diaphragms.

$$\overline{\boldsymbol{Z}}_{\mathrm{B}k} = \boldsymbol{T}_{k,d}^{-1} (\boldsymbol{T}_{k-1,d} \overline{\boldsymbol{Y}}_{\mathrm{A},k-1} \boldsymbol{T}_{k-1,d}^{-1})^{-1} \boldsymbol{T}_{k,d}. \tag{20}$$

The lower boundary of a section is always marked with A and the upper boundary with B. The transformation matrices $\boldsymbol{T}$ with a subscript d are partitioned matrices [10]. They contain only the rows associated with the discretization lines that are common to both regions. For special cases see [10] and [11].

2) Radial Waveguide Sections: In the more general case, the radial waveguide consists of concatenations of sections with different heights. We will obtain the solution for the fields in each of these sections by discretizing the equations in the longitudinal coordinate z. The discretization lines are shown in Fig. 2 and in more detail in Fig. 4. The discretization line numeration follows the positive z direction. The permittivity can be a function of z. Variations in r direction should be modeled by as many sections as necessary. The discretization for the kth section yields

$$\tilde{H}_\varphi \rightarrow \tilde{\mathbf{H}}_\varphi \tag{21}$$

$$E_z \rightarrow \mathbf{E}_z \tag{22}$$

$$\varepsilon_r \rightarrow \boldsymbol{\epsilon}_h, \boldsymbol{\epsilon}_e \tag{23}$$

$$\frac{\partial}{\partial \overline{z}} \rightarrow \overline{h}_z^{-1} \boldsymbol{D}_z = \overline{\boldsymbol{D}}_z. \tag{24}$$

H_φ and E_z are discretized on the same full lines. $\boldsymbol{\epsilon}_h$ denotes the diagonal matrix of the permittivities on these lines, $\boldsymbol{\epsilon}_e$ the diagonal matrix of the permittivities on the dashed lines. The difference operator matrix $\boldsymbol{D}_z$ has to fulfill the Neumann boundary conditions. Moreover, all the discretized quantities should be marked for the section k, which we do not write to avoid confusion. Again we perform a transformation with the matrix $\boldsymbol{T}_z$ to diagonalize the second order difference matrix according to

$$\tilde{\mathbf{H}}_\varphi = \boldsymbol{T}_z \overline{\mathbf{H}}_\varphi \qquad \boldsymbol{k}_r^2 = \boldsymbol{T}_z^{-1} (\boldsymbol{\epsilon}_h - \boldsymbol{\epsilon}_h \overline{\boldsymbol{D}}_z^t \boldsymbol{\epsilon}_e^{-1} \overline{\boldsymbol{D}}_z) \boldsymbol{T}_z. \tag{25}$$

The diagonal matrix $\boldsymbol{k}_r^2$ contains all eigenvalues and $\boldsymbol{T}_z$ corresponding eigenvectors of the total matrix in the parenthesis.

The discretized and diagonalized wave equation reduces to a Bessel equation

$$\frac{\partial}{\partial \overline{r}} \left(\overline{r}^{-1} \frac{\partial}{\partial \overline{r}} (\overline{r} \overline{\mathbf{H}}_\varphi) \right) + \boldsymbol{k}_r^2 \overline{\mathbf{H}}_\varphi = 0. \tag{26}$$

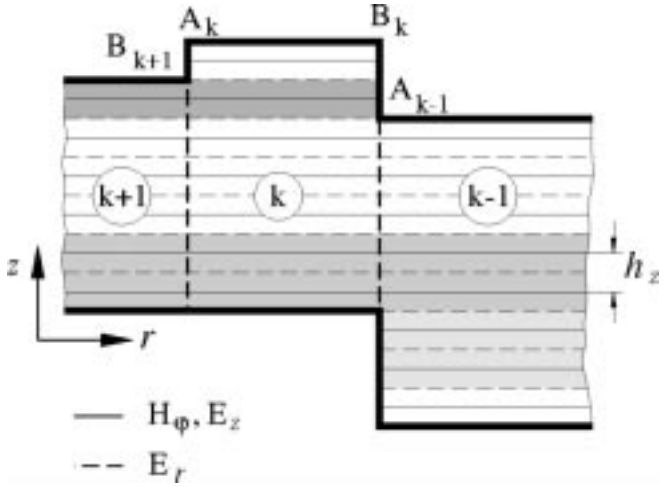

Fig. 4. Concatenations of the radial waveguide sections. The permittivities are functions of z.

Its general solution is expressed in terms of first-order Bessel and Neumann functions J_1 and Y_1

$$\overline{\mathbf{H}}_\varphi = J_1(\boldsymbol{k}_r\overline{r})\mathbf{A} + Y_1(\boldsymbol{k}_r\overline{r})\mathbf{B} \tag{27}$$

whose arguments contain the diagonal matrix $\boldsymbol{k}_r$. Therefore, $\mathcal{C}_1(\boldsymbol{k}_r\overline{r})$ ($\mathcal{C}$—general notation of cylindrical functions, J or Y) is also a diagonal matrix and will be abbreviated in the following by $\mathcal{C}_1$, namely, $\mathcal{C}_{1\mathrm{A}}$ if $\overline{r} = \overline{r}_\mathrm{A}$ or $\mathcal{C}_{1\mathrm{B}}$ if $\overline{r} = \overline{r}_\mathrm{B}$, e.g., $\boldsymbol{J}_{1\mathrm{B}} = J_1(\boldsymbol{k}_r\overline{r}_\mathrm{B})$. Using Hankel functions instead of Bessel and Neumann functions in (27), we can define the characteristic impedance matrix (normalized according to the free-space wave impedance η_0) for the wave propagation in forward direction (subscript f) at a position r ($\boldsymbol{H}^{(2)}_{0,1} = H^{(2)}_{0,1}(\boldsymbol{k}_r\overline{r})$) by

$$\overline{\mathbf{E}}_{zf} = \overline{\boldsymbol{Z}}_{r0}(-\overline{\mathbf{H}}_{\varphi f}) \qquad \overline{\boldsymbol{Z}}_{r0} = j\overline{\boldsymbol{\epsilon}}_h^{-1}\boldsymbol{k}_r\boldsymbol{H}^{(2)}_0(\boldsymbol{H}^{(2)}_1)^{-1}. \tag{28}$$

For $r \to \infty$ the characteristic impedance matrix approaches $\overline{\boldsymbol{Z}}_{r0} = \overline{\boldsymbol{\epsilon}}_h^{-1}\boldsymbol{k}_r$. For the fundamental mode and homogeneous dielectric we obtain $\overline{Z}_{r0} = 1/\sqrt{\epsilon_r}$. The relation between the electric and magnetic field components at the two section boundaries A and B is, again, given as a generalized two port relation by

$$\begin{bmatrix}\overline{\mathbf{E}}_{z\mathrm{A}}\\ \overline{\mathbf{E}}_{z\mathrm{B}}\end{bmatrix} = \begin{bmatrix}\overline{\boldsymbol{z}}_{\mathrm{AA}} & \overline{\boldsymbol{z}}_{\mathrm{AB}}\\ \overline{\boldsymbol{z}}_{\mathrm{BA}} & \overline{\boldsymbol{z}}_{\mathrm{BB}}\end{bmatrix}\begin{bmatrix}(-\overline{\mathbf{H}}_{\varphi\mathrm{A}})\\ -(-\overline{\mathbf{H}}_{\varphi\mathrm{B}})\end{bmatrix} \tag{29}$$

where

$$\overline{\boldsymbol{z}}_{\mathrm{AA}} = -j\overline{\boldsymbol{\epsilon}}_h^{-1}\boldsymbol{k}_r\boldsymbol{p}_1^{-1}\boldsymbol{q}_0 \qquad \overline{\boldsymbol{z}}_{\mathrm{AB}} = \frac{2}{\pi}(j\overline{r}_\mathrm{A}\boldsymbol{p}_1\overline{\boldsymbol{\epsilon}}_h)^{-1}$$
$$\overline{\boldsymbol{z}}_{\mathrm{BB}} = j\overline{\boldsymbol{\epsilon}}_h^{-1}\boldsymbol{k}_r\boldsymbol{p}_1^{-1}\boldsymbol{r}_0 \qquad \overline{\boldsymbol{z}}_{\mathrm{BA}} = \frac{2}{\pi}(j\overline{r}_\mathrm{B}\boldsymbol{p}_1\overline{\boldsymbol{\epsilon}}_h)^{-1} \tag{30}$$
$$\boldsymbol{p}_1 = \boldsymbol{J}_{1\mathrm{A}}\boldsymbol{Y}_{1\mathrm{B}} - \boldsymbol{J}_{1\mathrm{B}}\boldsymbol{Y}_{1\mathrm{A}} \qquad \overline{\boldsymbol{\epsilon}}_h = \boldsymbol{T}_z^{-1}\boldsymbol{\epsilon}_h\boldsymbol{T}_z \tag{31}$$

$\boldsymbol{p}_1$ being the generalized cross product of cylinder functions p_1 (see formula 9.1.32 in Abramowitz and Stegun [14]). In our case, $\boldsymbol{p}_1$ is a diagonal matrix containing $\boldsymbol{k}_r$ implicitly. In the same way the further generalized cross products of cylinder functions $\boldsymbol{p}_0$, $\boldsymbol{q}_0$, and $\boldsymbol{r}_0$ also correspond to the notations in formula 9.1.32 in [14] except that they are diagonal matrices.

In addition, the following relation for the general cylinder function $\mathcal{C}$ was used: $\mathcal{C}_0'(x) = -\mathcal{C}_1(x)$, $x = k_r\overline{r}$. Defining

$$\overline{\boldsymbol{E}}_{z\mathrm{A,B}} = \overline{\boldsymbol{Z}}_{\mathrm{A,B}}(-\overline{\boldsymbol{H}}_{\varphi\mathrm{A,B}}) \tag{32}$$

the impedance transfer from the output B of section k to its input A or vice versa yields

$$\overline{\boldsymbol{Z}}_\mathrm{A} = \overline{\boldsymbol{z}}_{\mathrm{AA}} - \overline{\boldsymbol{z}}_{\mathrm{AB}}(\overline{\boldsymbol{z}}_{\mathrm{BB}} + \overline{\boldsymbol{Z}}_\mathrm{B})^{-1}\overline{\boldsymbol{z}}_{\mathrm{BA}} \tag{33}$$
$$-\overline{\boldsymbol{Z}}_\mathrm{B} = \overline{\boldsymbol{z}}_{\mathrm{BB}} - \overline{\boldsymbol{z}}_{\mathrm{BA}}(\overline{\boldsymbol{z}}_{\mathrm{AA}} + (-\overline{\boldsymbol{Z}}_\mathrm{A}))^{-1}\overline{\boldsymbol{z}}_{\mathrm{AB}}. \tag{34}$$

The impedances $-\overline{\boldsymbol{Z}}_\mathrm{A}$ and $-\overline{\boldsymbol{Z}}_\mathrm{B}$ are the impedances for looking in $-r$ direction. Instead of (29), we may also use the inversion with the generalized y parameters

$$\overline{\boldsymbol{y}}_{\mathrm{AA}} = j\boldsymbol{k}_r^{-1}\boldsymbol{p}_0^{-1}\boldsymbol{r}_0\overline{\boldsymbol{\epsilon}}_h$$
$$\overline{\boldsymbol{y}}_{\mathrm{AB}} = j\frac{2}{\pi}(\boldsymbol{k}_r^2\overline{r}_\mathrm{A}\boldsymbol{p}_0)^{-1}\overline{\boldsymbol{\epsilon}}_h$$
$$\overline{\boldsymbol{y}}_{\mathrm{BB}} = -j\boldsymbol{k}_r^{-1}\boldsymbol{p}_0^{-1}\boldsymbol{q}_0\overline{\boldsymbol{\epsilon}}_h$$
$$\overline{\boldsymbol{y}}_{\mathrm{BA}} = j\frac{2}{\pi}(\boldsymbol{k}_r^2\overline{r}_\mathrm{B}\boldsymbol{p}_0)^{-1}\overline{\boldsymbol{\epsilon}}_h. \tag{35}$$

The $\overline{\boldsymbol{y}}$ and $\overline{\boldsymbol{z}}$ parameters are again introduced similar to network theory. With $\overline{\boldsymbol{Y}}_{\mathrm{A,B}} = \overline{\boldsymbol{Z}}_{\mathrm{A,B}}^{-1}$ the corresponding admittance transfer is analogous to the impedance transfer. The impedance transfer at concatenations of radial sections with offsets (e.g., between sections k and $k-1$ in Fig. 4) can again be performed with the general formula derived in [10] and reported in (20).

3) Study of Sections A, C, and E: In region A the solution must be an outgoing wave. The fields must be described by Hankel functions of the second kind. The regions C and E include the origin of the radial coordinate r. From the two parts of the general solution (27), only the first term is expressed by a well-behaved function. The second term possesses a singularity at the origin, but physically the fields should be finite. The special solutions for the regions A, C, and E in Fig. 2 are written as follows:

$$\begin{aligned}
\text{A:}\quad & \overline{\mathbf{H}}_\varphi = H_1^{(2)}(\boldsymbol{k}_{r\mathrm{A}}\overline{r})H_1^{(2)-1}(\boldsymbol{k}_{r\mathrm{A}}\overline{r}_0)\mathbf{A}_\mathrm{A} = -\overline{\boldsymbol{Y}}_\mathrm{A}\overline{\mathbf{E}}_z\\
& \overline{\mathbf{E}}_z = -j\overline{\boldsymbol{\epsilon}}_{h\mathrm{A}}^{-1}\boldsymbol{k}_{r\mathrm{A}}H_0^{(2)}(\boldsymbol{k}_{r\mathrm{A}}\overline{r})H_1^{(2)-1}(\boldsymbol{k}_{r\mathrm{A}}\overline{r}_0)\mathbf{A}_\mathrm{A}\\
\text{C:}\quad & \overline{\mathbf{H}}_\varphi = J_1(\boldsymbol{k}_{r\mathrm{C}}\overline{r})J_1^{-1}(\boldsymbol{k}_{r\mathrm{C}}\overline{r}_0)\mathbf{A}_\mathrm{C} = \overline{\boldsymbol{Y}}_\mathrm{C}\overline{\mathbf{E}}_z\\
& \overline{\mathbf{E}}_z = -j\overline{\boldsymbol{\epsilon}}_{h\mathrm{C}}^{-1}\boldsymbol{k}_{r\mathrm{C}}J_0(\boldsymbol{k}_{r\mathrm{C}}\overline{r})J_1^{-1}(\boldsymbol{k}_{r\mathrm{C}}\overline{r}_0)\mathbf{A}_\mathrm{C}\\
\text{E:}\quad & \overline{\mathbf{H}}_\varphi = J_1(\boldsymbol{k}_{r\mathrm{E}}\overline{r})J_1^{-1}(\boldsymbol{k}_{r\mathrm{E}}\overline{r}_i)\mathbf{A}_\mathrm{E} = \overline{\boldsymbol{Y}}_\mathrm{E}\overline{\mathbf{E}}_z\\
& \overline{\mathbf{E}}_z = -j\overline{\boldsymbol{\epsilon}}_{h\mathrm{E}}^{-1}\boldsymbol{k}_{r\mathrm{E}}J_0(\boldsymbol{k}_{r\mathrm{E}}\overline{r})J_1^{-1}(\boldsymbol{k}_{r\mathrm{E}}\overline{r}_i)\mathbf{A}_\mathrm{E}
\end{aligned} \tag{36}$$

where $H_1^{(2)}$ and $H_0^{(2)}$ are first- and zeroth-order Hankel functions of the second kind, respectively. These solutions are normalized so that the magnetic field components at $r = r_0$ or $r = r_i$ are given by $\mathbf{A}_\mathrm{A}$, $\mathbf{A}_\mathrm{C}$, and $\mathbf{A}_\mathrm{E}$, respectively. For open structures in z direction, as in regions A and C of Fig. 2, the operator $\overline{\boldsymbol{D}}_z$ in (24) has to be replaced by the operator $\overline{\boldsymbol{D}}_z^a$. This, in turn, requires introduction of absorbing boundary conditions (ABC).

We define the impedance matrices $\overline{\boldsymbol{Z}}_\mathrm{A} = \overline{\boldsymbol{Y}}_\mathrm{A}^{-1}$, $\overline{\boldsymbol{Z}}_\mathrm{C} = \overline{\boldsymbol{Y}}_\mathrm{C}^{-1}$, and $\overline{\boldsymbol{Z}}_\mathrm{E} = \overline{\boldsymbol{Y}}_\mathrm{E}^{-1}$ which are obtained from (36) (the signs are chosen according to the Poynting vector)

$$\overline{\boldsymbol{Z}}_\mathrm{A}(\overline{r}_0) = j\overline{\boldsymbol{\epsilon}}_{h\mathrm{A}}^{-1}\boldsymbol{k}_{r\mathrm{A}}H_0^{(2)}(\boldsymbol{k}_{r\mathrm{A}}\overline{r}_0)H_1^{(2)-1}(\boldsymbol{k}_{r\mathrm{A}}\overline{r}_0) \tag{37}$$
$$\overline{\boldsymbol{Z}}_\mathrm{C}(\overline{r}_0) = -j\overline{\boldsymbol{\epsilon}}_{h\mathrm{C}}^{-1}\boldsymbol{k}_{r\mathrm{C}}J_0(\boldsymbol{k}_{r\mathrm{C}}\overline{r}_0)J_1^{-1}(\boldsymbol{k}_{r\mathrm{C}}\overline{r}_0) \tag{38}$$

$$\overline{\boldsymbol{Z}}_{\mathrm{E}}(\overline{r}_i) = -j\overline{\epsilon}_{h\mathrm{E}}^{-1}\boldsymbol{k}_{r\mathrm{E}}J_0(\boldsymbol{k}_{r\mathrm{E}}\overline{r}_i)J_1^{-1}(\boldsymbol{k}_{r\mathrm{E}}\overline{r}_i). \tag{39}$$

4) Radiation Impedance at the Aperture B: The impedance $\overline{\boldsymbol{Z}}_{\mathrm{B}}$ (see Fig. 2), which is defined as in (32) is obtained from the matching process at $\overline{r} = \overline{r}_0$. Matching the electric and magnetic fields, we obtain

$$\mathbf{E}_{z\mathrm{A}} = \begin{bmatrix} \mathbf{E}_{z\mathrm{B}} \\ \mathbf{E}_{z\mathrm{M}} \\ \mathbf{E}_{z\mathrm{C}} \end{bmatrix} \qquad \mathbf{H}_{\varphi\mathrm{A}} = \begin{bmatrix} \mathbf{H}_{\varphi\mathrm{B}} \\ \mathbf{J}_{\mathrm{M}} \\ \mathbf{H}_{\varphi\mathrm{C}} \end{bmatrix}. \tag{40}$$

The subvector $\mathbf{E}_{z\mathrm{M}}$ represents the electric field on the nonideal surface of the metallic cylinder with $r = r_0$ between regions B and C. For ideal metal $\mathbf{E}_{z\mathrm{M}}$ must be a vector with zero components. $\mathbf{J}_{\mathrm{M}}$ being the current density on the same places as $\mathbf{E}_{z\mathrm{M}}$. For the vectors in transformed domain the equation for the electric field reads as

$$\boldsymbol{T}_{\mathrm{A}}\overline{\mathbf{E}}_{z\mathrm{A}} = \begin{bmatrix} \boldsymbol{T}_{\mathrm{AB}} \\ \boldsymbol{T}_{\mathrm{AM}} \\ \boldsymbol{T}_{\mathrm{AC}} \end{bmatrix} \overline{\mathbf{E}}_{z\mathrm{A}} = \begin{bmatrix} \boldsymbol{T}_{\mathrm{B}}\overline{\mathbf{E}}_{z\mathrm{B}} \\ \mathbf{E}_{z\mathrm{M}} \\ \boldsymbol{T}_{\mathrm{C}}\overline{\mathbf{E}}_{z\mathrm{C}} \end{bmatrix} \tag{41}$$

where $\boldsymbol{T}_{\mathrm{AB}}$, $\boldsymbol{T}_{\mathrm{AC}}$, and $\boldsymbol{T}_{\mathrm{AM}}$ are parts of $\boldsymbol{T}_{\mathrm{A}}$ associated with the regions B, C, and metallization, respectively, obtained by matrix partition technique proposed in [10].

The vector $\overline{\mathbf{E}}_{z\mathrm{A}}$ as function of $\overline{\mathbf{E}}_{z\mathrm{B}}$, $\overline{\mathbf{E}}_{z\mathrm{M}}$, and $\overline{\mathbf{E}}_{z\mathrm{C}}$, therefore, can be written in the following form using the corresponding partition parts of $\boldsymbol{T}_{\mathrm{A}}^{-1}$:

$$\overline{\mathbf{E}}_{z\mathrm{A}} = \boldsymbol{T}_{\mathrm{AB}}^{-1}\boldsymbol{T}_{\mathrm{B}}\overline{\mathbf{E}}_{z\mathrm{B}} + \boldsymbol{T}_{\mathrm{AC}}^{-1}\boldsymbol{T}_{\mathrm{C}}\overline{\mathbf{E}}_{z\mathrm{C}} + \boldsymbol{T}_{\mathrm{AM}}^{-1}\mathbf{E}_{z\mathrm{M}}. \tag{42}$$

The equation for the magnetic field in the transform domain has an analogous form as (41) and splits into

$$\boldsymbol{T}_{\mathrm{B}}\overline{\mathbf{H}}_{\varphi\mathrm{B}} = \boldsymbol{T}_{\mathrm{AB}}\overline{\mathbf{H}}_{\varphi\mathrm{A}} \tag{43}$$

$$\boldsymbol{T}_{\mathrm{C}}\overline{\mathbf{H}}_{\varphi\mathrm{C}} = \boldsymbol{T}_{\mathrm{AC}}\overline{\mathbf{H}}_{\varphi\mathrm{A}} \tag{44}$$

$$\mathbf{J}_{\mathrm{M}} = \boldsymbol{T}_{\mathrm{AM}}\overline{\mathbf{H}}_{\varphi\mathrm{A}}. \tag{45}$$

Replacing $\overline{\mathbf{H}}_{\varphi\mathrm{A}}$ in (43)–(45) by $-\overline{\boldsymbol{Y}}_{\mathrm{A}}\overline{\mathbf{E}}_{z\mathrm{A}}$ and introducing (42) into these equations we obtain

$$\begin{bmatrix} -\overline{\mathbf{H}}_{\varphi\mathrm{B}} \\ -\overline{\mathbf{H}}_{\varphi\mathrm{C}} \\ -\mathbf{J}_{\mathrm{M}} \end{bmatrix} = \begin{bmatrix} \overline{\boldsymbol{y}}_{\mathrm{BB}} & \overline{\boldsymbol{y}}_{\mathrm{BC}} & \overline{\boldsymbol{y}}_{\mathrm{BM}} \\ \overline{\boldsymbol{y}}_{\mathrm{CB}} & \overline{\boldsymbol{y}}_{\mathrm{CC}} & \overline{\boldsymbol{y}}_{\mathrm{CM}} \\ \overline{\boldsymbol{y}}_{\mathrm{MB}} & \overline{\boldsymbol{y}}_{\mathrm{MC}} & \overline{\boldsymbol{y}}_{\mathrm{MM}} \end{bmatrix} \begin{bmatrix} \overline{\mathbf{E}}_{z\mathrm{B}} \\ \overline{\mathbf{E}}_{z\mathrm{C}} \\ \mathbf{E}_{z\mathrm{M}} \end{bmatrix} \tag{46}$$

with, e.g.,

$$\overline{\boldsymbol{y}}_{\mathrm{CB}} = \boldsymbol{T}_{\mathrm{C}}^{-1}\boldsymbol{T}_{\mathrm{AC}}\overline{\boldsymbol{Y}}_{\mathrm{A}}\boldsymbol{T}_{\mathrm{AB}}^{-1}\boldsymbol{T}_{\mathrm{B}}. \tag{47}$$

The other submatrices are obtained in an analogous manner. We first consider the case of ideal material with $\mathbf{E}_{z\mathrm{M}} = \mathbf{0}$. The last equation in system (46) decouples from the first ones in this case. Now with respect to (36) and (38) we get from the second equation in (46)

$$\overline{\mathbf{E}}_{z\mathrm{C}} = -(\overline{\boldsymbol{Y}}_{\mathrm{C}} + \overline{\boldsymbol{y}}_{\mathrm{CC}})^{-1}\overline{\boldsymbol{y}}_{\mathrm{CB}}\overline{\mathbf{E}}_{z\mathrm{B}} \tag{48}$$

which may be introduced into the first equation in (46)

$$-\overline{\mathbf{H}}_{\varphi\mathrm{B}} = (\overline{\boldsymbol{y}}_{\mathrm{BB}} - \overline{\boldsymbol{y}}_{\mathrm{BC}}(\overline{\boldsymbol{Y}}_{\mathrm{C}} + \overline{\boldsymbol{y}}_{\mathrm{CC}})^{-1}\overline{\boldsymbol{y}}_{\mathrm{CB}})\overline{\mathbf{E}}_{z\mathrm{B}}. \tag{49}$$

The admittance $\overline{\boldsymbol{Y}}_{\mathrm{B}}$ is, therefore, given by

$$\overline{\boldsymbol{Y}}_{\mathrm{B}} = \overline{\boldsymbol{y}}_{\mathrm{BB}} - \overline{\boldsymbol{y}}_{\mathrm{BC}}(\overline{\boldsymbol{Y}}_{\mathrm{C}} + \overline{\boldsymbol{y}}_{\mathrm{CC}})^{-1}\overline{\boldsymbol{y}}_{\mathrm{CB}} \tag{50}$$

which has the same form as (17).

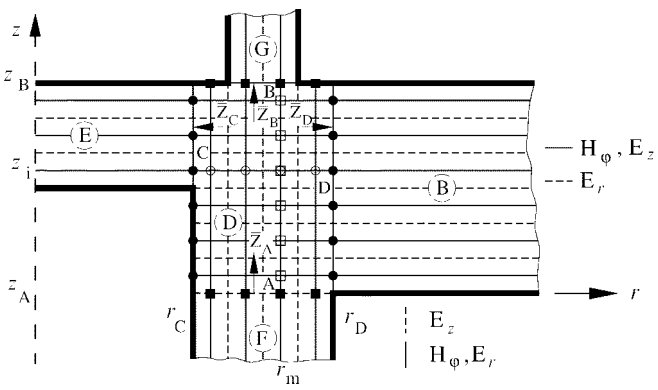

Fig. 5. General region with crossed discretization lines.

In the case of nonideal metal wall (especially for the monopole analysis), we use the approximate boundary conditions for the tangential fields on the metallic surface $\eta_m\vec{H}_t = \vec{e}_r \times \vec{E}_t$, which results in

$$\mathbf{J}_{z\mathrm{M}} = \frac{\eta_0}{\eta_m}\mathbf{E}_{z\mathrm{M}} = \boldsymbol{Y}_{\mathrm{M}}\mathbf{E}_{z\mathrm{M}}. \tag{51}$$

$\boldsymbol{Y}_{\mathrm{M}}$ being a diagonal matrix with the elements η_0/η_m. η_m is the wave impedance in the lossy material with the conductivity κ and is given by $\eta_m = \sqrt{jk_0\eta_0/\kappa}$. We have to use new parameters $\overline{\boldsymbol{y}}_{\mathrm{UV}}^{\mathrm{n}}$ instead of $\overline{\boldsymbol{y}}_{\mathrm{UV}}$ (U, V = B, C) in (48)–(50). Replacing $\mathbf{E}_{z\mathrm{M}}$ in the first two equations of (46) by $\mathbf{E}_{z\mathrm{M}}$ obtained from the last one yields

$$\overline{\boldsymbol{y}}_{\mathrm{UV}}^{\mathrm{n}} = \overline{\boldsymbol{y}}_{\mathrm{UV}} - \overline{\boldsymbol{y}}_{\mathrm{UM}}(\boldsymbol{Y}_{\mathrm{M}} + \overline{\boldsymbol{y}}_{\mathrm{MM}})^{-1}\overline{\boldsymbol{y}}_{\mathrm{MV}}. \tag{52}$$

Let us assume that the antenna is fed by the fundamental mode of the radial waveguide then the field $\overline{\mathbf{E}}_{\mathrm{B}}$ is known and with that and the admittance $\overline{\boldsymbol{Y}}_{\mathrm{B}}$ we can calculate the fields $\overline{\mathbf{E}}_{z\mathrm{C}}$ and $\overline{\mathbf{H}}_{\varphi\mathrm{B}}$ by (48) and (49), respectively, and then the other quantities by (46), especially the surface current density $\mathbf{J}_{\mathrm{M}}$.

5) Regions with Crossed Lines: As shown in Fig. 2 the region D has interfaces with regions of radial (regions F and G) and z discretization (regions B and E). To describe the fields in region D we use the linear combination

$$H_{\varphi}^{\mathrm{D}} = H_{\varphi r}^{\mathrm{D}} + H_{\varphi z}^{\mathrm{D}}. \tag{53}$$

The two parts are discretized on different discretization line systems crossing each other at 90°. The second subscript denotes the discretization direction. In Fig. 5, the general region with crossed lines is sketched. In vertical direction this region is bounded by the planes A and B at z_{A} and z_{B} and in radial direction by surfaces C and D at r_{C} and r_{D}, respectively. The four surfaces of the region D are like four generalized ports. Our goal is to obtain a general relation between the fields at these four ports. We have to determine the field parts belonging to the vertical discretization lines at the ports C and D and the field parts belonging to the horizontal discretization lines at the ports A and B.

6) Field Part Related to Discretization in r Direction: We assume in the first step that ε_r is a constant. For the part with discretization in r direction we can adapt the solution obtained in Section II-B.1 [see (14)].

$$\begin{bmatrix} \overline{\mathbf{H}}_{\varphi r\mathrm{A}} \\ -\overline{\mathbf{H}}_{\varphi r\mathrm{B}} \end{bmatrix} = \widehat{\overline{\boldsymbol{y}}}_{\mathrm{AB}} \begin{bmatrix} \overline{\mathbf{E}}_{r r\mathrm{A}} \\ \overline{\mathbf{E}}_{r r\mathrm{B}} \end{bmatrix}. \tag{54}$$

The matrix of y-parameter matrices is abbreviated by $\hat{\hat{\boldsymbol{y}}}_{\mathrm{AB}}$. All quantities have to be marked with a sub- or superscript D for region D, which is omitted here. For the z dependence of magnetic field we may write ($z = 0$ in plane A: $z_A = 0$)

$$\overline{\mathbf{H}}_{\varphi r}(z) = \frac{\sinh(\boldsymbol{\Gamma}(\overline{H} - \overline{z}))}{\sinh(\boldsymbol{\Gamma}\overline{H})}\,\overline{\mathbf{H}}_{\varphi r\mathrm{A}} + \frac{\sinh(\boldsymbol{\Gamma}\overline{z})}{\sinh(\boldsymbol{\Gamma}\overline{H})}\,\overline{\mathbf{H}}_{\varphi r\mathrm{B}} \quad (55)$$

where $\overline{H} = k_0(z_{\mathrm{B}} - z_{\mathrm{A}})$. The diagonal matrix $\sinh(\boldsymbol{\Gamma}\overline{H})$ in the denominator really needs to be inverted. This equation must now be discretized for z values of discretization lines in r direction. At such a position z_i (see Fig. 5), we may write

$$\overline{\mathbf{H}}_{\varphi r}(z_i) = \boldsymbol{\Lambda}^d_{\mathrm{A}i}\overline{\mathbf{H}}_{\varphi r\mathrm{A}} + \boldsymbol{\Lambda}^d_{\mathrm{B}i}\overline{\mathbf{H}}_{\varphi r\mathrm{B}} \quad (56)$$

with diagonal matrices $\boldsymbol{\Lambda}^d_i$ given by the expressions

$$\boldsymbol{\Lambda}^d_{\mathrm{A}i} = \sinh(\boldsymbol{\Gamma}(\overline{H} - \overline{z}_i))(\sinh(\boldsymbol{\Gamma}\overline{H}))^{-1} \quad (57)$$

$$\boldsymbol{\Lambda}^d_{\mathrm{B}i} = \sinh(\boldsymbol{\Gamma}\overline{z}_i)(\sinh(\boldsymbol{\Gamma}\overline{H}))^{-1}. \quad (58)$$

The vector $\mathbf{H}_{\varphi r}(z_i) = \boldsymbol{T}_r\overline{\mathbf{H}}_{\varphi r}(z_i)$ then gives the values $H_{\varphi r}$ in the points marked by circles $\circ$ in Fig. 5. For the matching procedure we need the values of the field at the boundaries $r = r_{\mathrm{C}}$ and $r = r_{\mathrm{D}}$. Because of the Neumann conditions we must extrapolate from points near the boundary to the boundary. This can easily be done by the transformation matrix $\boldsymbol{T}_r$ (see Appendix). We obtain at the position z_i on the left (R $\equiv$ C, $r = r_{\mathrm{C}}$) or right (R $\equiv$ D, $r = r_{\mathrm{D}}$) boundary (marked by $\bullet$ at the surfaces C and D)

$$H_{\varphi r\mathrm{R}}(z_i) = \mathbf{T}_{r\Delta\mathrm{R}}(\boldsymbol{\Lambda}^d_{\mathrm{A}i}\overline{\mathbf{H}}_{\varphi r\mathrm{A}} + \boldsymbol{\Lambda}^d_{\mathrm{B}i}\overline{\mathbf{H}}_{\varphi r\mathrm{B}}). \quad (59)$$

$\mathbf{T}_{r\Delta\mathrm{R}}$ is a row vector constructed from weighted first (last) rows of the matrix $\boldsymbol{T}_r$ (see Appendix). If we want to change the order of $\mathbf{T}_{r\Delta\mathrm{R}}$ and $\boldsymbol{\Lambda}^d_i$ we must also change these quantities in a suitable matrix form. $\mathbf{T}_{r\Delta\mathrm{R}}$ should then be formed as a diagonal matrix $\boldsymbol{T}^d_{r\Delta\mathrm{R}}$ and $\boldsymbol{\Lambda}^d_i$—as a row vector $\boldsymbol{\Lambda}_i$. By doing this, the result can be written for all values z_i simultaneously

$$\mathbf{H}_{\varphi r\mathrm{R}} = \boldsymbol{\Lambda}_{\mathrm{A}}\boldsymbol{T}^d_{r\Delta\mathrm{R}}\overline{\mathbf{H}}_{\varphi r\mathrm{A}} + \boldsymbol{\Lambda}_{\mathrm{B}}\boldsymbol{T}^d_{r\Delta\mathrm{R}}\overline{\mathbf{H}}_{\varphi r\mathrm{B}} \quad (60)$$

where the full matrices $\boldsymbol{\Lambda}_{\mathrm{A}}$ and $\boldsymbol{\Lambda}_{\mathrm{B}}$ are given by

$$(\boldsymbol{\Lambda}_{\mathrm{A}})_{ik} = \sinh(\boldsymbol{\Gamma}_k(\overline{H} - \overline{z}_i))(\sinh(\boldsymbol{\Gamma}_k\overline{H}))^{-1} \quad (61)$$

$$(\boldsymbol{\Lambda}_{\mathrm{B}})_{ik} = \sinh(\boldsymbol{\Gamma}_k\overline{z}_i)(\sinh(\boldsymbol{\Gamma}_k\overline{H}))^{-1}. \quad (62)$$

In transformed domain, we therefore have

$$\overline{\mathbf{H}}_{\varphi r\mathrm{R}} = \boldsymbol{T}_z^{-1}\boldsymbol{\Lambda}_{\mathrm{A}}\boldsymbol{T}^d_{r\Delta\mathrm{R}}\overline{\mathbf{H}}_{\varphi r\mathrm{A}} + \boldsymbol{T}_z^{-1}\boldsymbol{\Lambda}_{\mathrm{B}}\boldsymbol{T}^d_{r\Delta\mathrm{R}}\overline{\mathbf{H}}_{\varphi r\mathrm{B}}. \quad (63)$$

The relations between the magnetic field parts discretized in r direction at the four ports A, B, C, and D can now be expressed in the following matrix form:

$$\begin{bmatrix} (-\overline{\mathbf{H}}_{\varphi r\mathrm{C}}) \\ -(-\overline{\mathbf{H}}_{\varphi r\mathrm{D}}) \end{bmatrix} = \underbrace{\begin{bmatrix} \overline{\boldsymbol{V}}_{\mathrm{CA}} & \overline{\boldsymbol{V}}_{\mathrm{CB}} \\ \overline{\boldsymbol{V}}_{\mathrm{DA}} & \overline{\boldsymbol{V}}_{\mathrm{DB}} \end{bmatrix}}_{\hat{\hat{\boldsymbol{V}}}^{\mathrm{CD}}_{\mathrm{AB}}} \begin{bmatrix} \overline{\boldsymbol{H}}_{\varphi r\mathrm{A}} \\ -\overline{\boldsymbol{H}}_{\varphi r\mathrm{B}} \end{bmatrix} \quad (64)$$

where

$$\overline{\boldsymbol{V}}_{\mathrm{CA}} = -\boldsymbol{T}_z^{-1}\boldsymbol{\Lambda}_{\mathrm{A}}\boldsymbol{T}^d_{r\Delta\mathrm{C}} \qquad \overline{\boldsymbol{V}}_{\mathrm{CB}} = \boldsymbol{T}_z^{-1}\boldsymbol{\Lambda}_{\mathrm{B}}\boldsymbol{T}^d_{r\Delta\mathrm{C}}$$

$$\overline{\boldsymbol{V}}_{\mathrm{DB}} = -\boldsymbol{T}_z^{-1}\boldsymbol{\Lambda}_{\mathrm{B}}\boldsymbol{T}^d_{r\Delta\mathrm{D}} \qquad \overline{\boldsymbol{V}}_{\mathrm{DA}} = \boldsymbol{T}_z^{-1}\boldsymbol{\Lambda}_{\mathrm{A}}\boldsymbol{T}^d_{r\Delta\mathrm{D}}. \quad (65)$$

From the part $\overline{\mathbf{H}}_{\varphi r}$ we do not obtain an E_z component on both sides of region D because of the Dirichlet boundary conditions for this component.

7) Field Part Related to Discretization in z Direction: To derive a relation for the field parts related to discretization in z direction at ports A and B from those at ports C and D in Fig. 5 we adapt the solutions in Section II-B.2. The (29) reads for the surfaces C and D and the field parts under investigation

$$\begin{bmatrix} (-\overline{\mathbf{H}}_{\varphi z\mathrm{C}}) \\ -(-\overline{\mathbf{H}}_{\varphi z\mathrm{D}}) \end{bmatrix} = \hat{\hat{\boldsymbol{y}}}_{\mathrm{CD}} \begin{bmatrix} \overline{\mathbf{E}}_{zz\mathrm{C}} \\ \overline{\mathbf{E}}_{zz\mathrm{D}} \end{bmatrix} \quad (66)$$

where the submatrices of $\hat{\hat{\boldsymbol{y}}}_{\mathrm{CD}}$ are obtained from (35) by exchanging the subscripts A and B by C and D, respectively. All quantities have to be marked with a sub- or superscript D for region D, which is omitted here. To derive a suitable formula for fields at arbitrary radii, we can adapt the general solution in (27), which we write in the following form:

$$\overline{\mathbf{H}}_{\varphi z}(r) = [J_1(\boldsymbol{k}_r\overline{r}) \quad Y_1(\boldsymbol{k}_r\overline{r})] \begin{bmatrix} \mathbf{A} \\ \mathbf{B} \end{bmatrix}. \quad (67)$$

For the surfaces C and D we obtain

$$\begin{bmatrix} \overline{\mathbf{H}}_{\varphi z\mathrm{C}} \\ \overline{\mathbf{H}}_{\varphi z\mathrm{D}} \end{bmatrix} = \begin{bmatrix} J_1(\boldsymbol{k}_r\overline{r}_{\mathrm{C}}) & Y_1(\boldsymbol{k}_r\overline{r}_{\mathrm{C}}) \\ J_1(\boldsymbol{k}_r\overline{r}_{\mathrm{D}}) & Y_1(\boldsymbol{k}_r\overline{r}_{\mathrm{D}}) \end{bmatrix} \begin{bmatrix} \mathbf{A} \\ \mathbf{B} \end{bmatrix}. \quad (68)$$

The inversion yields

$$\begin{bmatrix} \mathbf{A} \\ \mathbf{B} \end{bmatrix} = \hat{\boldsymbol{p}}_1^{-1} \begin{bmatrix} Y_1(\boldsymbol{k}_r\overline{r}_{\mathrm{D}}) & -Y_1(\boldsymbol{k}_r\overline{r}_{\mathrm{C}}) \\ -J_1(\boldsymbol{k}_r\overline{r}_{\mathrm{D}}) & J_1(\boldsymbol{k}_r\overline{r}_{\mathrm{C}}) \end{bmatrix} \begin{bmatrix} \overline{\mathbf{H}}_{\varphi z\mathrm{C}} \\ \overline{\mathbf{H}}_{\varphi z\mathrm{D}} \end{bmatrix} \quad (69)$$

in view of ([14, formula 9.1.32])

$$\boldsymbol{p}_1^{\mathrm{CD}} = J_1(\boldsymbol{k}_r\overline{r}_{\mathrm{C}})Y_1(\boldsymbol{k}_r\overline{r}_{\mathrm{D}}) - Y_1(\boldsymbol{k}_r\overline{r}_{\mathrm{C}})J_1(\boldsymbol{k}_r\overline{r}_{\mathrm{D}}). \quad (70)$$

The superscripts (C and D) at $\boldsymbol{p}_1$ here and in the following denote the radii which have to be introduced into the arguments of the cylinder functions. The order of the superscripts is the same as the order of the radii in the functions.

Introducing (69) into (67), we therefore obtain for position $r = r_m$ similarly to (56)

$$\overline{\mathbf{H}}_{\varphi z}(\overline{r}_m) = \boldsymbol{\Lambda}^d_{\mathrm{C}m}\overline{\mathbf{H}}_{\varphi z\mathrm{C}} + \boldsymbol{\Lambda}^d_{\mathrm{D}m}\overline{\mathbf{H}}_{\varphi z\mathrm{D}} \quad (71)$$

with

$$\boldsymbol{\Lambda}^d_{\mathrm{C}m} = \boldsymbol{p}_1^{m\mathrm{D}}(\boldsymbol{p}_1^{\mathrm{CD}})^{-1} \qquad \boldsymbol{\Lambda}^d_{\mathrm{D}m} = \boldsymbol{p}_1^{\mathrm{C}m}(\boldsymbol{p}_1^{\mathrm{CD}})^{-1}. \quad (72)$$

The vector $\mathbf{H}_{\varphi z}(\overline{r}_m) = \boldsymbol{T}_z\overline{\mathbf{H}}_{\varphi z}(\overline{r}_m)$ then gives the values $H_{\varphi z}$ in the points marked by empty squares $\square$ in Fig. 5. The values at the transition points (marked by full squares $\blacksquare$) in planes A (R $\equiv$ A) and B (R $\equiv$ B) are again obtained by an analogous process. The following equation holds:

$$\mathbf{H}_{\varphi z\mathrm{R}} = \boldsymbol{\Lambda}_{\mathrm{C}}\boldsymbol{T}^d_{z\Delta\mathrm{R}}\overline{\mathbf{H}}_{\varphi z\mathrm{C}} + \boldsymbol{\Lambda}_{\mathrm{D}}\boldsymbol{T}^d_{z\Delta\mathrm{R}}\overline{\mathbf{H}}_{\varphi z\mathrm{D}} \quad (73)$$

where $\boldsymbol{\Lambda}_{\mathrm{C}}$ and $\boldsymbol{\Lambda}_{\mathrm{D}}$ are full matrices. They are constructed analogous $\boldsymbol{\Lambda}_{\mathrm{A,\,B}}$ in (61) and (62)

$$(\boldsymbol{\Lambda}_{\mathrm{C}})_{mn} = p_1^{m\mathrm{D}}/p_1^{\mathrm{CD}} \qquad (\boldsymbol{\Lambda}_{\mathrm{D}})_{mn} = p_1^{\mathrm{C}m}/p_1^{\mathrm{CD}}. \quad (74)$$

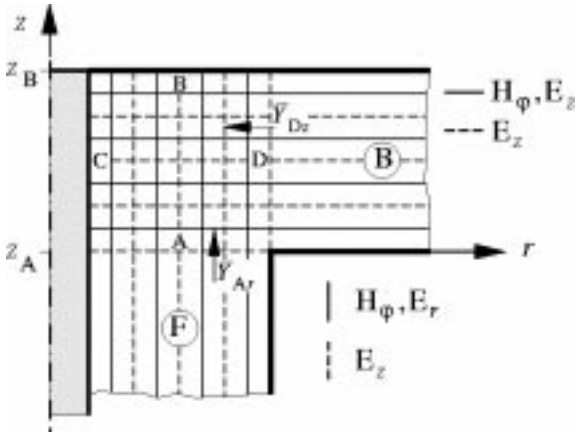

Fig. 6. Transition section with crossed lines.

In the argument of the cylinder functions the nth component of $\boldsymbol{k}_r$ has to be introduced. The general solution is

$$\begin{bmatrix} \overline{\mathbf{H}}_{\varphi z\mathrm{A}} \\ -\overline{\mathbf{H}}_{\varphi z\mathrm{B}} \end{bmatrix} \underbrace{\begin{bmatrix} \overline{\boldsymbol{V}}_{\mathrm{AC}} & \overline{\boldsymbol{V}}_{\mathrm{AD}} \\ \overline{\boldsymbol{V}}_{\mathrm{BC}} & \overline{\boldsymbol{V}}_{\mathrm{BD}} \end{bmatrix}}_{\widehat{\overline{\boldsymbol{V}}}_{\mathrm{CD}}^{\mathrm{AB}}} \begin{bmatrix} (-\overline{\mathbf{H}}_{\varphi z\mathrm{C}}) \\ -(-\overline{\mathbf{H}}_{\varphi z\mathrm{D}}) \end{bmatrix} \tag{75}$$

where

$$\begin{aligned} \overline{\mathbf{V}}_{\mathrm{AC}} &= -\boldsymbol{T}_r^{-1}\boldsymbol{\Lambda}_{\mathrm{C}}\boldsymbol{T}_{z\Delta\mathrm{A}}^{d} & \overline{\mathbf{V}}_{\mathrm{AD}} &= \boldsymbol{T}_r^{-1}\boldsymbol{\Lambda}_{\mathrm{D}}\boldsymbol{T}_{z\Delta\mathrm{A}}^{d} \\ \overline{\mathbf{V}}_{\mathrm{BD}} &= -\boldsymbol{T}_r^{-1}\boldsymbol{\Lambda}_{\mathrm{D}}\boldsymbol{T}_{z\Delta\mathrm{B}}^{d} & \overline{\mathbf{V}}_{\mathrm{BC}} &= \boldsymbol{T}_r^{-1}\boldsymbol{\Lambda}_{\mathrm{C}}\boldsymbol{T}_{z\Delta\mathrm{B}}^{d}. \end{aligned} \tag{76}$$

Again, the field extrapolation to planes A and B is performed by the diagonal matrices $\boldsymbol{T}_{\Delta z\mathrm{A}}^{d}$ and $\boldsymbol{T}_{\Delta z\mathrm{B}}^{d}$.

8) Special Case I—Region D with Short Circuited Ports B and C: In this subsection, we assume that the ports B and C are short circuited. The region D now transforms the waves from coaxial line directly to the radial parallel plate transmission line. In Fig. 6, this transition region is shown with some details. In this special case, we have a short circuit on the upper side (plane or port B) of this region. Therefore, we obtain as input admittance for this field part

$$\overline{\boldsymbol{Y}}_{\mathrm{A}r} = \overline{\boldsymbol{y}}_1 = \boldsymbol{Y}_{0z}(\tanh(\boldsymbol{\Gamma}_z\overline{H}))^{-1} \tag{77}$$

with $\boldsymbol{Y}_{0z}$ given by to (13). The magnetic field part at port D from field part $\mathbf{H}_{\varphi r}$ at port A is given by

$$\overline{\mathbf{H}}_{\varphi r\mathrm{D}} = \overline{\boldsymbol{V}}_{\mathrm{DA}}\overline{\mathbf{H}}_{\varphi r\mathrm{A}} \qquad \overline{\boldsymbol{V}}_{\mathrm{DA}} = \boldsymbol{T}_z^{-1}\boldsymbol{\Lambda}_{\mathrm{A}}\boldsymbol{T}_{r\Delta\mathrm{D}}^{d} \tag{78}$$

where

$$(\boldsymbol{\Lambda}_{\mathrm{A}})_{ik} = \cosh(\boldsymbol{\Gamma}_k(\overline{H} - \overline{z}_i))(\cosh(\boldsymbol{\Gamma}_k\overline{H}))^{-1}. \tag{79}$$

The surface (or port) C on the left side is a short circuit.

The expression for the admittance $\overline{\boldsymbol{Y}}_{\mathrm{D}z}$ becomes

$$\overline{\boldsymbol{Y}}_{\mathrm{D}z} = -j\boldsymbol{k}_r^{-1}\boldsymbol{p}_0^{-1}\boldsymbol{s}_0^{-1}\boldsymbol{p}_1\boldsymbol{q}_0\bar{\epsilon}_h. \tag{80}$$

The radii to be introduced in (80) are $\overline{r}_{\mathrm{C}}$ and $\overline{r}_{\mathrm{D}}$. We obtain the field relation $\overline{\mathbf{H}}_{\varphi z}(\overline{r}_m) = \boldsymbol{\Lambda}_{\mathrm{D}}\overline{\mathbf{H}}_{\varphi z\mathrm{D}}$ with

$$\boldsymbol{\Lambda}_{\mathrm{D}} = (\boldsymbol{p}_1^{\mathrm{CD}})^{-1}\left(\boldsymbol{p}_1^{\mathrm{C}m} + \frac{2}{\pi}(\boldsymbol{k}_r\overline{r}_{\mathrm{C}}\boldsymbol{q}_0)^{-1}\boldsymbol{p}_1^{m\mathrm{D}}\right) \tag{81}$$

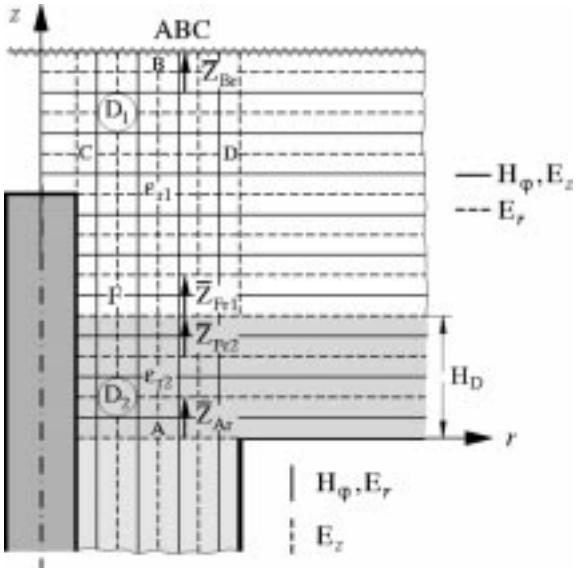

Fig. 7. Region D with multilayered dielectric.

inserting $\mathbf{E}_{zz\mathrm{C}} = 0$ in the general equation. Thus, we obtain for the magnetic field part at port A

$$\overline{\mathbf{H}}_{\varphi z\mathrm{A}} = \boldsymbol{T}_r^{-1}\boldsymbol{\Lambda}_{\mathrm{D}}\boldsymbol{T}_{\Delta z\mathrm{A}}\overline{\mathbf{H}}_{\varphi z\mathrm{D}} = \overline{\boldsymbol{V}}_{\mathrm{AD}}\overline{\mathbf{H}}_{\varphi z\mathrm{D}}. \tag{82}$$

9) Special Case II—Region D with Layered Dielectric: In Fig. 7, the situation with two dielectric layers is given. The region D now has to be subdivided into two subregions D_1 and D_2. In comparison to the general case, only the situation in z direction has been changed. Therefore, we will give only the formulas for this direction. The magnetic field resulting from part $\mathbf{H}_{\varphi r}$ must be determined at an arbitrary z_i by the field $\mathbf{H}_{\varphi r\mathrm{A}}$. Taking into account the ABC's in plane B or—which is identical in this case—assuming an infinite height of region D_1 the following results are valid

$$\overline{\boldsymbol{Z}}_{\mathrm{B}r} = \overline{\boldsymbol{Z}}_{\mathrm{Fr}_1} = \overline{\boldsymbol{Z}}_{01} = -j\varepsilon_{r1}^{-1}\boldsymbol{\Gamma}_1. \tag{83}$$

The magnetic field depends in the following way of z_i

$$\overline{\mathbf{H}}_{\varphi r} = e^{-\boldsymbol{\Gamma}_1(\overline{z}_i - \overline{z}_{\mathrm{F}})}\overline{\mathbf{H}}_{\varphi r\mathrm{F}}. \tag{84}$$

In region D_2 we adapt the general solution (14)

$$\begin{bmatrix} \overline{\mathbf{E}}_{rr\mathrm{A}} \\ \overline{\mathbf{E}}_{rr\mathrm{F}} \end{bmatrix} = \begin{bmatrix} \overline{\boldsymbol{z}}_1 & \overline{\boldsymbol{z}}_2 \\ \overline{\boldsymbol{z}}_2 & \overline{\boldsymbol{z}}_1 \end{bmatrix}_{|\mathrm{D}_2} \begin{bmatrix} \overline{\mathbf{H}}_{\varphi r\mathrm{A}} \\ -\overline{\mathbf{H}}_{\varphi r\mathrm{F}} \end{bmatrix}. \tag{85}$$

Introducing $\overline{\mathbf{E}}_{rr\mathrm{F}} = \overline{\boldsymbol{Z}}_{01}\overline{\mathbf{H}}_{\varphi r\mathrm{F}}$ into the second equation of system (85) we obtain

$$\overline{\mathbf{H}}_{\varphi r\mathrm{F}} = (\boldsymbol{Z}_{01} + \overline{\boldsymbol{z}}_1)^{-1}\overline{\boldsymbol{z}}_2\overline{\mathbf{H}}_{\varphi r\mathrm{A}} = \overline{\boldsymbol{V}}_{\mathrm{FA}}\overline{\mathbf{H}}_{\varphi r\mathrm{A}} \tag{86}$$

$$\overline{\boldsymbol{V}}_{\mathrm{FA}} = (\cosh(\boldsymbol{\Gamma}_2\overline{H}_{\mathrm{D}}) + \overline{\boldsymbol{Z}}_{01}\overline{\boldsymbol{Z}}_{02}^{-1}\sinh(\boldsymbol{\Gamma}_2\overline{H}_{\mathrm{D}}))^{-1}. \tag{87}$$

The first equation in (85) yields

$$\overline{\boldsymbol{Z}}_{\mathrm{A}r} = \overline{\boldsymbol{z}}_1 - \overline{\boldsymbol{z}}_2(\boldsymbol{Z}_{01} + \overline{\boldsymbol{z}}_1)^{-1}\overline{\boldsymbol{z}}_2 = \overline{\boldsymbol{z}}_1 - \overline{\boldsymbol{z}}_2\overline{\boldsymbol{V}}_{\mathrm{FA}}. \tag{88}$$

Now, instead of (60) we can write

$$\mathbf{H}_{\varphi r\mathrm{R}} = \begin{bmatrix} \boldsymbol{\Lambda}_{\mathrm{A}} + \boldsymbol{\Lambda}_{\mathrm{F}2}\overline{\boldsymbol{V}}_{\mathrm{FA}} \\ \boldsymbol{\Lambda}_{\mathrm{F}1}\overline{\boldsymbol{V}}_{\mathrm{FA}} \end{bmatrix}\overline{\boldsymbol{T}}_{r\Delta\mathrm{R}}^{d}\overline{\mathbf{H}}_{\varphi r\mathrm{A}} \tag{89}$$

where

$$(\mathbf{\Lambda}_{\mathrm{A}})_{ik} = \sinh(\mathbf{\Gamma}_{2k}(\overline{H}_{\mathrm{D}} - \overline{z}_i))(\sinh(\mathbf{\Gamma}_{2k}\overline{H}_{\mathrm{D}}))^{-1} \quad (90)$$

$$(\mathbf{\Lambda}_{\mathrm{F}_2})_{ik} = \sinh(\mathbf{\Gamma}_{2k}\overline{z}_i)(\sinh(\mathbf{\Gamma}_{2k}\overline{H}_{\mathrm{D}}))^{-1} \quad (91)$$

$$(\mathbf{\Lambda}_{\mathrm{F}_1})_{ik} = e^{-\mathbf{\Gamma}_{1k}(\overline{z}_i - \overline{H}_{\mathrm{D}})}. \quad (92)$$

In (90) and (91) i runs for the position $\overline{\boldsymbol{z}}_i$ in region D_2 and in (92) for the position $\overline{\boldsymbol{z}}_i$ in D_1. The analogous equations to (64) are

$$\begin{bmatrix} \overline{\mathbf{H}}_{\varphi r\mathrm{C}} \\ \overline{\mathbf{H}}_{\varphi r\mathrm{D}} \end{bmatrix} = \begin{bmatrix} \overline{\boldsymbol{V}}_{\mathrm{CA}} \\ \overline{\boldsymbol{V}}_{\mathrm{DA}} \end{bmatrix} \overline{\mathbf{H}}_{\varphi r\mathrm{A}} \quad (93)$$

with

$$\overline{\boldsymbol{V}}_{\mathrm{CA}} = \boldsymbol{T}_z^{-1} \begin{bmatrix} \mathbf{\Lambda}_{\mathrm{A}} + \mathbf{\Lambda}_{\mathrm{F2}}\overline{\boldsymbol{V}}_{\mathrm{FA}} \\ \mathbf{\Lambda}_{\mathrm{F1}}\overline{\boldsymbol{V}}_{\mathrm{FA}} \end{bmatrix} \boldsymbol{T}^d_{r\Delta\mathrm{C}} \quad (94)$$

$$\overline{\boldsymbol{V}}_{\mathrm{DA}} = \boldsymbol{T}_z^{-1} \begin{bmatrix} \mathbf{\Lambda}_{\mathrm{A}} + \mathbf{\Lambda}_{\mathrm{F2}}\overline{\boldsymbol{V}}_{\mathrm{FA}} \\ \mathbf{\Lambda}_{\mathrm{F1}}\overline{\boldsymbol{V}}_{\mathrm{FA}} \end{bmatrix} \boldsymbol{T}^d_{r\Delta\mathrm{D}}. \quad (95)$$

It should be noted that the antenna in Figs. 1(c) and 7 can also be analyzed using only the concept described in Section II-B.1, that means with discretization lines only in z direction. The sections above the ground plane must have a much greater radius than the coaxial line and ABC's must be introduced at the outer wall.

C. Port Relations of Section D

In this chapter, the results in previous sections will be collected to for a general relation between the fields at the four ports A, B, C, and D of Section D in Fig. 5. Then, e.g., the input impedance/admittance of one port can be calculated from the known load impedance/admittance of the other ports by means of this general relation. We have derived four systems of equations: (54), (64), (66), and (75). We have only one tangential part for the E field at each port. Therefore, we may abbreviate in the following way:

$$\overline{\mathbf{E}}_{r\mathrm{A,\,B}} = \overline{\mathbf{E}}_{\mathrm{A,\,B}} \qquad \overline{\mathbf{E}}_{z\mathrm{C,\,D}} = \overline{\mathbf{E}}_{\mathrm{C,\,D}}. \quad (96)$$

The H field parts have to be added

$$\mathbf{H}_{\varphi\mathrm{R}} = \mathbf{H}_{\varphi z\mathrm{R}} + \mathbf{H}_{\varphi r\mathrm{R}} = \mathbf{H}_{\mathrm{R}} \qquad \mathrm{R} = \mathrm{A,\ B,\ C,\ or\ D.} \quad (97)$$

This can also be done in the transform domain. Introducing (54) in (64) and (66) in (75) and adding according to (97), we obtain in compact form as

$$\begin{bmatrix} \overline{\mathbf{H}}_{\mathrm{AB}} \\ -\overline{\mathbf{H}}_{\mathrm{CD}} \end{bmatrix} = \begin{bmatrix} \widehat{\overline{\boldsymbol{y}}}_{\mathrm{AB}} & \widehat{\overline{\boldsymbol{y}}}^{\mathrm{AB}}_{\mathrm{CD}} \\ \widehat{\overline{\boldsymbol{y}}}^{\mathrm{CD}}_{\mathrm{AB}} & \widehat{\overline{\boldsymbol{y}}}_{\mathrm{CD}} \end{bmatrix} \begin{bmatrix} \overline{\mathbf{E}}_{\mathrm{AB}} \\ \overline{\mathbf{E}}_{\mathrm{CD}} \end{bmatrix} \quad (98)$$

where

$$\widehat{\overline{\boldsymbol{y}}}^{\mathrm{CD}}_{\mathrm{AB}} = \widehat{\overline{\boldsymbol{V}}}^{\mathrm{CD}}_{\mathrm{AB}} \widehat{\overline{\boldsymbol{y}}}_{\mathrm{AB}} \qquad \widehat{\overline{\boldsymbol{y}}}^{\mathrm{AB}}_{\mathrm{CD}} = \widehat{\overline{\boldsymbol{V}}}^{\mathrm{AB}}_{\mathrm{CD}} \widehat{\overline{\boldsymbol{y}}}_{\mathrm{CD}} \quad (99)$$

and

$$\overline{\mathbf{H}}_{\mathrm{AB,\,CD}} = \begin{bmatrix} \overline{\mathbf{H}}_{\mathrm{A,\,C}} \\ -\overline{\mathbf{H}}_{\mathrm{B,\,D}} \end{bmatrix} \qquad \overline{\mathbf{E}}_{\mathrm{AB,\,CD}} = \begin{bmatrix} \overline{\mathbf{E}}_{\mathrm{A,\,C}} \\ \overline{\mathbf{E}}_{\mathrm{B,\,D}} \end{bmatrix}. \quad (100)$$

Equation (98) is a general port relation. Knowing the sources and the loads all the fields at ports can be calculated. Let us assume that port A is the port connected with the waveguide from the source (coaxial feed line). Then the impedance matrices $\overline{\boldsymbol{Z}}_{\mathrm{B}}$, $\overline{\boldsymbol{Z}}_{\mathrm{C}}$, $\overline{\boldsymbol{Z}}_{\mathrm{D}}$ defined by

$$\begin{aligned} \overline{\mathbf{E}}_{r\mathrm{A}} &= \overline{\boldsymbol{Z}}_{\mathrm{A}}\overline{\mathbf{H}}_{\varphi\mathrm{A}} \qquad & \overline{\mathbf{E}}_{z\mathrm{C}} &= \overline{\boldsymbol{Z}}_{\mathrm{C}}\overline{\mathbf{H}}_{\varphi\mathrm{C}} \\ \overline{\mathbf{E}}_{r\mathrm{B}} &= \overline{\boldsymbol{Z}}_{\mathrm{B}}\overline{\mathbf{H}}_{\varphi\mathrm{B}} \qquad & \overline{\mathbf{E}}_{z\mathrm{D}} &= \overline{\boldsymbol{Z}}_{\mathrm{D}}(-\overline{\mathbf{H}}_{\varphi\mathrm{D}}) \end{aligned} \quad (101)$$

are the load impedance matrices. They are defined inside the region D and are obtained from the impedance matrices of the connecting waveguides by a transformation according to (20) from the admittances of the neighboring regions B, E, and D. $\overline{\boldsymbol{Y}}_{\mathrm{C}}$, e.g., is calculated from $\overline{\boldsymbol{Z}}_{\mathrm{E}}$ in (39) using transformation formula (20). The input impedance matrix $\overline{\boldsymbol{Z}}_{\mathrm{A}}$ has to be determined from (98). Then the load impedance matrix of the coaxial fed line has to be calculated by (20).

The solution may be obtained by the following algorithm. Equation (98) has to be inverted. We combine also the port impedance matrices in the following way:

$$\hat{\overline{\boldsymbol{Z}}}_{\mathrm{AB}} = \mathrm{Diag}(\overline{\boldsymbol{Z}}_{\mathrm{A}}, -\overline{\boldsymbol{Z}}_{\mathrm{B}}) \qquad \hat{\overline{\boldsymbol{Z}}}_{\mathrm{CD}} = \mathrm{Diag}(\overline{\boldsymbol{Z}}_{\mathrm{C}}, \overline{\boldsymbol{Z}}_{\mathrm{D}}). \quad (102)$$

Then the combined impedance matrix $\hat{\overline{\boldsymbol{Z}}}_{\mathrm{AB}}$ can be calculated in the known and usual way. In a second step, the impedance matrix $\overline{\boldsymbol{Z}}_{\mathrm{A}}$ can obtained in an analogous manner.

For the special cases I and II we will give explicit formulas. In the special case I, the total fields at ports A and D in transform domain are given by

$$\begin{bmatrix} \overline{\mathbf{H}}_{\varphi\mathrm{A}} \\ \overline{\mathbf{H}}_{\varphi\mathrm{D}} \end{bmatrix} = \begin{bmatrix} \boldsymbol{I}_r & \overline{\boldsymbol{V}}_{\mathrm{AD}} \\ \overline{\boldsymbol{V}}_{\mathrm{DA}} & \boldsymbol{I}_z \end{bmatrix} \begin{bmatrix} \overline{\mathbf{H}}_{\varphi\mathrm{rA}} \\ \overline{\mathbf{H}}_{\varphi\mathrm{zD}} \end{bmatrix}. \quad (103)$$

$\overline{\mathbf{H}}_{\varphi\mathrm{rA}}$ and $\overline{\mathbf{H}}_{\varphi\mathrm{zD}}$ may now be replaced by $\overline{\mathbf{E}}_{\mathrm{rA}}$ and $\overline{\mathbf{E}}_{\mathrm{zD}}$, respectively, with the help of the admittances in (77) and (80), respectively

$$\begin{bmatrix} \overline{\mathbf{H}}_{\varphi\mathrm{A}} \\ \overline{\mathbf{H}}_{\varphi\mathrm{D}} \end{bmatrix} = \begin{bmatrix} \overline{\boldsymbol{Y}}_{\mathrm{Ar}} & \overline{\boldsymbol{V}}_{\mathrm{AD}}\overline{\boldsymbol{Y}}_{\mathrm{Dz}} \\ \overline{\boldsymbol{V}}_{\mathrm{DA}}\overline{\boldsymbol{Y}}_{\mathrm{Ar}} & \overline{\boldsymbol{Y}}_{\mathrm{Dz}} \end{bmatrix} \begin{bmatrix} \overline{\mathbf{E}}_{r\mathrm{A}} \\ \overline{\mathbf{E}}_{z\mathrm{D}} \end{bmatrix}. \quad (104)$$

With the load admittance in plane D (input admittance of the radial waveguide Section II-B) defined by

$$\overline{\mathbf{E}}_{\mathrm{zD}} = -\overline{\mathbf{Y}}_{\mathrm{D}}\overline{\mathbf{H}}_{\varphi\mathrm{D}} \quad (105)$$

we get from (104) the total input admittance in plane A by

$$\overline{\boldsymbol{Y}}_{\mathrm{A}} = \overline{\boldsymbol{Y}}_{\mathrm{A}r} - \overline{\boldsymbol{V}}_{\mathrm{AD}}\overline{\boldsymbol{Y}}_{\mathrm{Dz}}(\overline{\boldsymbol{Y}}_{\mathrm{D}} + \overline{\boldsymbol{Y}}_{\mathrm{Dz}})^{-1}\overline{\boldsymbol{V}}_{\mathrm{DA}}\overline{\boldsymbol{Y}}_{\mathrm{A}r}. \quad (106)$$

If in the transition plane from coaxial line to region D there is a step in diameters (e.g., if an diaphragm is introduced in that plane), a further transformation according to (20) is necessary to obtain the load admittance of the coaxial line.

For the special case II, we obtain from (66), (75), (88), and (93) in a similar procedure as in the general case by adding the magnetic field parts at the ports the following three-port relation:

$$\begin{bmatrix} \overline{\mathbf{H}}_{\varphi\mathrm{A}} \\ (-\overline{\mathbf{H}}_{\varphi\mathrm{C}}) \\ -(-\overline{\mathbf{H}}_{\varphi\mathrm{D}}) \end{bmatrix} = \begin{bmatrix} \overline{\boldsymbol{Y}}_{\mathrm{A}r} & \overline{\boldsymbol{Y}}_{\mathrm{AC}} & \overline{\boldsymbol{Y}}_{\mathrm{AD}} \\ \overline{\boldsymbol{Y}}_{\mathrm{CA}} & \overline{\boldsymbol{y}}_{\mathrm{CC}} & \overline{\boldsymbol{y}}_{\mathrm{CD}} \\ \overline{\boldsymbol{Y}}_{\mathrm{DA}} & \overline{\boldsymbol{y}}_{\mathrm{DC}} & \overline{\boldsymbol{y}}_{\mathrm{DD}} \end{bmatrix} \begin{bmatrix} \overline{\mathbf{E}}_{r\mathrm{A}} \\ \overline{\mathbf{E}}_{z\mathrm{C}} \\ \overline{\mathbf{E}}_{z\mathrm{D}} \end{bmatrix} \quad (107)$$

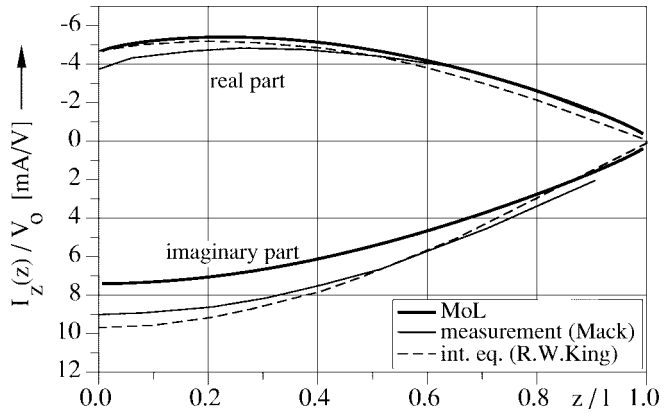

Fig. 8. Current distribution on one stub of a $\lambda/2$ dipole antenna. For dimensions see Fig. 9. The results for comparison are taken from Collin–Zucker [15].

where the following abbreviations are used:

$$\begin{aligned}
\overline{\boldsymbol{Y}}_{\mathrm{AC}} &= -\overline{\boldsymbol{V}}_{\mathrm{AC}}\overline{\boldsymbol{y}}_{\mathrm{CC}} + \overline{\boldsymbol{V}}_{\mathrm{AD}}\overline{\boldsymbol{y}}_{\mathrm{DC}} \\
\overline{\boldsymbol{Y}}_{\mathrm{AD}} &= -\overline{\boldsymbol{V}}_{\mathrm{AC}}\overline{\boldsymbol{y}}_{\mathrm{CD}} + \overline{\boldsymbol{V}}_{\mathrm{AD}}\overline{\boldsymbol{y}}_{\mathrm{DD}} \\
\overline{\boldsymbol{Y}}_{\mathrm{CA}} &= -\overline{\boldsymbol{V}}_{\mathrm{CA}}\overline{\boldsymbol{Y}}_{\mathrm{A}r} \\
\overline{\boldsymbol{Y}}_{\mathrm{DA}} &= \overline{\boldsymbol{V}}_{\mathrm{DA}}\overline{\boldsymbol{Y}}_{\mathrm{A}r}.
\end{aligned} \tag{108}$$

We introduce the impedance $\overline{\boldsymbol{Z}}_{\mathrm{C}}$ according to $\overline{\mathbf{E}}_{z\mathrm{C}} = \overline{\boldsymbol{Z}}_{\mathrm{C}}\overline{\mathbf{H}}_{\varphi\mathrm{C}}$ where

$$\overline{\boldsymbol{Z}}_{\mathrm{C}} = \boldsymbol{T}_{\mathrm{DE}}^{-1}\boldsymbol{T}_{\mathrm{E}}\overline{\boldsymbol{Z}}_{E}\boldsymbol{T}_{\mathrm{E}}^{-1}\boldsymbol{T}_{\mathrm{DE}} \tag{109}$$

with the reduced matrix $\boldsymbol{T}_{\mathrm{D}}$ according to the region E yielding $\boldsymbol{T}_{\mathrm{DE}}$. $\overline{\boldsymbol{Z}}_{\mathrm{E}}$ and $\boldsymbol{T}_{\mathrm{E}}$ have to be computed with ABC's on the upper side of region E. Then we obtain the two port relation

$$\begin{bmatrix} \overline{\mathbf{H}}_{\varphi\mathrm{A}} \\ -(-\overline{\mathbf{H}}_{\varphi\mathrm{D}}) \end{bmatrix} = \begin{bmatrix} \overline{\boldsymbol{y}}^{\mathrm{n}}_{\mathrm{AA}} & \overline{\boldsymbol{y}}^{\mathrm{n}}_{\mathrm{AD}} \\ \overline{\boldsymbol{y}}^{\mathrm{n}}_{\mathrm{DA}} & \overline{\boldsymbol{y}}^{\mathrm{n}}_{\mathrm{DD}} \end{bmatrix} \begin{bmatrix} \overline{\mathbf{E}}_{r\mathrm{A}} \\ \overline{\mathbf{E}}_{z\mathrm{D}} \end{bmatrix}. \tag{110}$$

We obtain from the last equation the input admittance

$$\overline{\boldsymbol{Y}}_{\mathrm{A}} = \overline{\boldsymbol{y}}^{\mathrm{n}}_{\mathrm{AA}} - \overline{\boldsymbol{y}}^{\mathrm{n}}_{\mathrm{AD}}(\overline{\boldsymbol{Y}}_{\mathrm{D}} + \overline{\boldsymbol{y}}^{\mathrm{n}}_{\mathrm{DD}})^{-1}\overline{\boldsymbol{y}}^{\mathrm{n}}_{\mathrm{DA}} \tag{111}$$

with the load admittance $\overline{\boldsymbol{Y}}_{\mathrm{D}}$ according to (105).

III. Numerical Results

Illustrative numerical results for some example structures are presented. In the first example, results for dipole antenna is presented. Fig. 8 shows the current distribution. The current distribution for a λ dipole is given in [16] obtained with a slightly different algorithm. In the results by the MoL the finite radius of the antenna is taken into account. Therefore, the values at the end are not zero as it is also the case in the measured results of Mack taken from Collin–Zucker [15]. The results of R. W. King also taken from Collin–Zucker [15] are obtained by an integral equation method. The radius of the dipole stubs are assumed to be approximately zero. In Fig. 9 the diagram for the input impedance of the dipole obtained from the field in the gap between the stubs and the input current is drawn. Curves a, b, and c for three different gaps of increasing values are shown. The impedance in the series

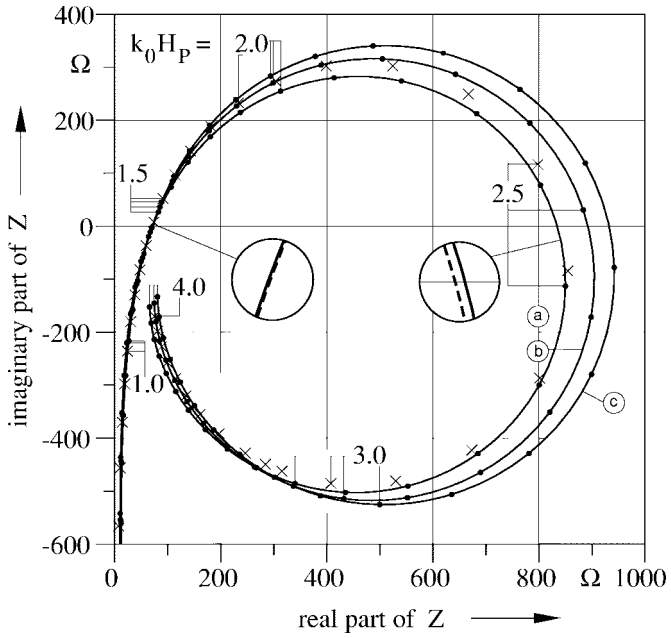

Fig. 9. Input impedance loci of a dipole antenna parametrized with $k_0 H$ (k_0 = free-space wave number): ——— lossless, - - - with loss, × results from King.

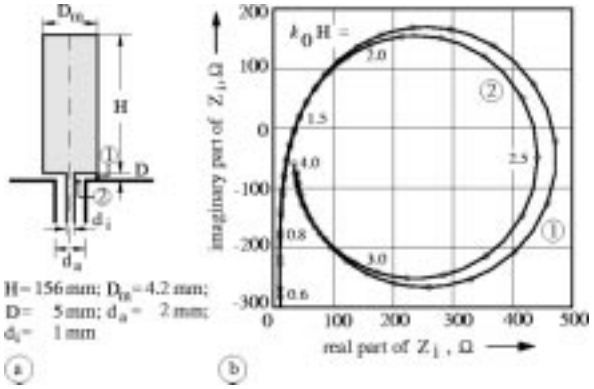

Fig. 10. Input impedance of a coaxial line-fed monopole antenna at two different positions. (a) Sketch of the antenna with dimensions. (b) Input impedance in the complex plane.

resonance in all three cases is about 71 Ω. Taking into account losses for the dipole of copper with $\kappa = 56\ \Omega^{-1}$ m/mm^2 the dashed curve was achieved. The loss resistance has the value of 0.023 Ω in the series type equivalent circuit for the $2H = \lambda/2$ dipole and the value of 39, 9.6, and 6.2 MΩ in the parallel type equivalent circuit for the $2H = \lambda$ dipole. In the next example, results for a coaxial line fed monopole antenna are plotted in Fig. 10. The antenna input impedance for two different places is plotted in the complex plane. Place (1) is in the outer gap side of the monopole and the ground, place (2) is on the end of the coaxial feed line. The diagram shows the well-known spiral behavior. The first real input impedance has a value of about 36.6 Ω.

In Fig. 11, results for the input impedances on a Smith chart of a monopole partially buried in a grounded dielectric substrate. These results are obtained with 115 discretization lines in horizontal direction (65 in region C) and 45 in

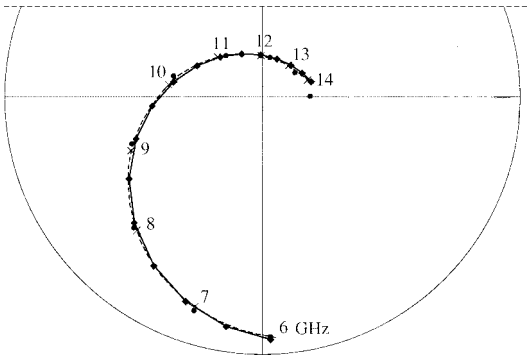

Fig. 11. Input impedance on a Smith chart of the monopole partly buried in a dielectric substrate with the dimensions given in [17]: ∘ ——— ∘ MoL, × – – – × numerical results of [17], • • • experimental results of [19].

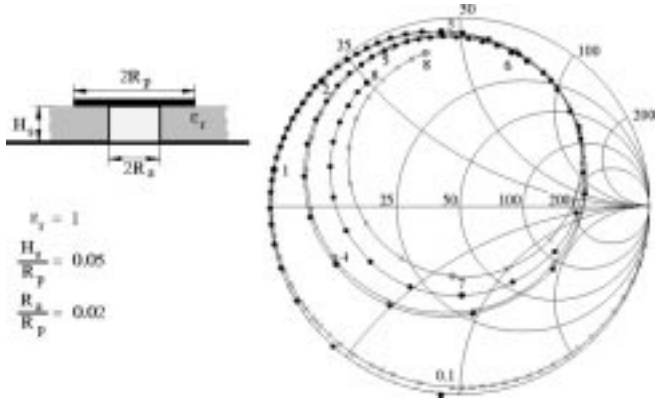

Fig. 12. Input impedance of a planar circular antenna at $r = R_a$ on a Smith chart. Parameter $k_0 R_p$ (k_0 = free-space wave number): • – – – • results from [20].

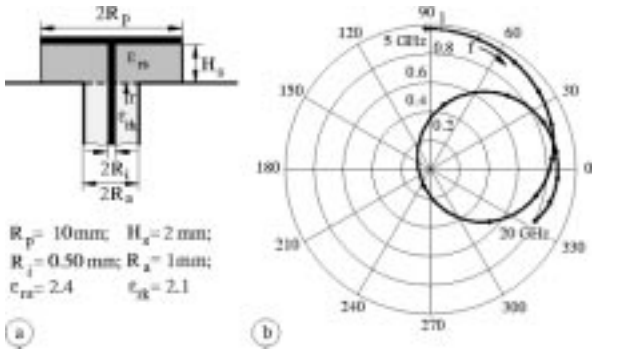

Fig. 13. Reflection coefficient S_{11} of a coaxial line-fed circular patch antenna at the marked position. (a) Sketch of the antenna with dimensions. (b) Reflection coefficient in the complex plane.

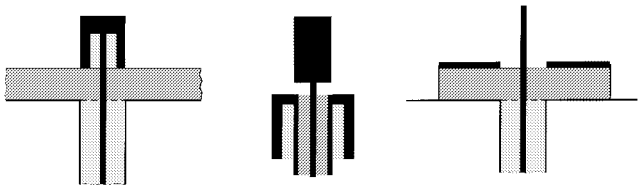

Fig. 14. Other forms of axially symmetric antennas.

the coaxial line. For a convergence investigation concerning the crossed discretization lines (see [3]). Numerical results obtained with the modal expansion method [17] are given for comparison. Also measured values reported by Alexopoulos [19] are introduced. All results are in very good agreement. In Fig. 12, the input impedance of a centered microstrip disk antenna is plotted in a Smith chart with a center impedance of 50 Ω. The parameter is $k_0 R_p$. For comparison, the result from [20] obtained by the moment-method solution are given. Up to $k_0 R_p \approx 6.5$ there is a quite good agreement. Apart from discretization no approximations are introduced in the MoL. Fig. 13(b) is a plot in polar coordinates of the input reflection coefficient for the circular patch antenna sketched in Fig. 13(a). The antenna is fed by a coaxial line. Further elements can be introduced in the feed line, e.g., to match the input impedance.

IV. Other Structures

The analysis procedure can be modified in a suitable way to enable investigations of circular patch antennas with feed line positioned outside the center and rectangular patch antennas. In this case, a discretization also in φ direction is necessary.

The algorithm can also be used for studying various transitions between coaxial and parallel plate lines. The described algorithm can also be used to investigate the effect of finite ground metallization with radius r_{M}. The region A then has to be interpreted as a radial line which transforms the impedance from the aperture at r_{M}. The procedure for calculation of the impedance at $r = r_{\mathrm{M}}$ is completely analogous to that at $r = r_0$ described in Section II-B.4. The Fig. 14 shows other forms of axially symmetric antennas.

V. Conclusions

A general method is proposed for the efficient analysis of general axially symmetric antennas. The algorithm is analogous to the well-known transmission line theory but using as many as necessary modes in each of the sections in the structure. The modes are obtained by the method of lines. To maintain the impedance/admittance transfer from the load to the input adequate transfer relations for the different sections are developed and written in similar forms. A special section is that where waveguide sections of different direction are concatenated. Here, crossed lines are introduced (this should not be "mixed up" with two-dimensional discretization). The determination of the field should be done in reverse direction. Starting at the source and using the impedances/admittances calculated before the fields can be successively calculated from section to section analogous as in a multilayered waveguide cross section described in [10]. The far field of the antenna can be obtained from the tangential fields on the surrounding area of the device by the usual near-field/far-field transformation and from that the radiation pattern can be extracted. This transformation is well developed. To improve the accuracy a further partition especially of the region A as described in Section II can be introduced. In principle, all necessary formulas are given for this case. For radial discretization ABC's have to be introduced on the outer side.

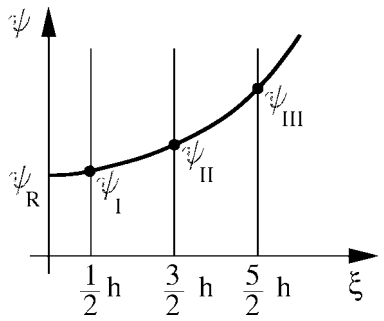

Fig. 15. Field behavior in case of Neumann boundary condition.

APPENDIX
FIELD EXTRAPOLATIONS FOR NEUMANN BOUNDARY CONDITIONS

For the analysis algorithms developed in the previous sections, we need the fields at the boundaries in case of Neumann boundary conditions. We consider an arbitrary function $\psi(\xi)$. Let ξ be a coordinate perpendicular to the boundary. The first discretization line in the vicinity of the boundary is at distance $\frac{1}{2}h$ from it (see Fig. 15). We must extrapolate from the neighboring discretization lines. The field behavior is of approximately parabolic form. Introducing

$$\psi = \psi_{\mathrm{R}} + a\left(\frac{\xi}{h}\right)^2 \tag{112}$$

we obtain from the values ψ_{I} and ψ_{II} on the lines at $\xi = \frac{1}{2}h$ and $\xi = \frac{3}{2}h$ on the boundary

$$\psi_{\mathrm{R}} = \tfrac{9}{8}\psi_{\mathrm{I}} - \tfrac{1}{8}\psi_{\mathrm{II}}. \tag{113}$$

For the discretized field we have $\boldsymbol{\psi} = \boldsymbol{T}\overline{\boldsymbol{\psi}}$. For the values on the boundaries we therefore obtain $\psi_{\mathrm{R}}(y) = \mathbf{T}_{\Delta\mathrm{R}}\overline{\boldsymbol{\psi}}(y)$ where $\mathbf{T}_{\Delta\mathrm{R}}$ depends on the boundary side (R $\equiv$ A: side where discretization starts, R $\equiv$ B: side where discretization ends). Explicitly, we have

$$\mathbf{T}_{\Delta\mathrm{A}} = \tfrac{1}{8}(9\mathbf{T}_1 - \mathbf{T}_2) \qquad \mathbf{T}_{\Delta\mathrm{B}} = \tfrac{1}{8}(9\mathbf{T}_{\mathrm{N}} - \mathbf{T}_{\mathrm{N}-1}) \tag{114}$$

on start site of discretization and end, respectively. $\mathbf{T}_1$ and $\boldsymbol{T}_2$ ($\mathbf{T}_{\mathrm{N}}$ and $\mathbf{T}_{\mathrm{N}-1}$) are the first (last) and the second (last but one) row vector of $\boldsymbol{T}$.

In general, we must assume that the curve contains a linear term. We need now a further discretization line (ψ_{III}) and a further row of $\boldsymbol{T}$. The new row vectors $\boldsymbol{T}_{\Delta\mathrm{R}}$ are given by

$$\mathbf{T}_{\Delta\mathrm{A,B}} = \tfrac{1}{8}(15\mathbf{T}_{1,\mathrm{N}} - 10\mathbf{T}_{2,\mathrm{N}-1} + 3\mathbf{T}_{3,\mathrm{N}-2}). \tag{115}$$

REFERENCES

[1] R. Pregla and W. Pascher, "The method of lines," in *Numerical Techniques for Microwave and Millimeter Wave Passive Structures*, T. Itoh, Ed. New York: Wiley, 1989, pp. 381–446.

[2] R. Pregla, "MoL-BPM method of lines based beam propagation method," in *Methods for Modeling and Simulation of Guided-Wave Optoelectronic Devices*, W. P. Huang, Ed. Cambridge, MA: EMW, 1995; PIER 11 in *Progress Electromagn. Res.*, pp. 51–102.

[3] W. Pascher and R. Pregla, "Analysis of rectangular waveguide junctions by the method of lines," *IEEE Trans. Microwave Theory Tech.*, vol. 43, pp. 2649–2653, Dec. 1995.

[4] ——, "Vectorial analysis of bends in optical strip waveguides by the method of lines," *Radio Sci.*, vol. 28, pp. 1229–1233, 1993.

[5] U. Rogge and R. Pregla, "Method of lines for the analysis of strip-loaded optical waveguides," *J. Opt. Soc. Amer. B*, vol. 8, no. 2, pp. 459–463, Feb. 1991.

[6] D. Kremer and R. Pregla, "The method of lines for the hybrid analysis of multilayered dielectric resonators," in *IEEE MTT-S Int. Symp. Dig.*, Orlando, FL, May 1995, pp. 491–494.

[7] R. Pregla, "The method of lines for the unified analysis of microstrip and dielectric waveguides," *Electromagn.*, vol. 15, no. 5, pp. 441–456, 1995.

[8] ——, "The method of lines for modeling of integrated optics structures," in *Latsis Symp. Computat. Electromagn.*, Zürich, Switzerland, Sept. 1995, pp. 216–229.

[9] ——, "General formulas for the method of lines in cylindrical coordinates," *IEEE Trans. Microwave Theory Tech.*, vol. 43, pp. 1617–1620, July 1995.

[10] ——, "The method of lines as generalized transmission line technique for the analysis of multilayered structures," *AEÜ*, vol. 50, no. 5, pp. 293–300, Sept. 1996.

[11] ——, "Concatenations of waveguide sections," *Proc. Inst. Elect. Eng. Microwave Antennas Propagat.*, vol. 144, pt. H, no. 2, pp. 119–125, Apr. 1997.

[12] R. Pregla and L. Vietzorreck, "Calculation of input impedances of planar antennas with the method of lines," in *Proc. Progress in Electromagn. Res. Symp. (PIERS)*, Noordwijk, The Netherlands, July 1994, pp. CD-ROM.

[13] L. Vietzorreck and R. Pregla, "Modeling of planar and conformal antennas by the method of lines," in *Inform. Technische Gesellschaft-Fachtagung*, Starnberg, Germany, Apr. 1996, pp. 141–144.

[14] M. Abramowitz and I. A. Stegun, *Handbook of Mathematical Functions.* New York: Dover, 1965, ch. 9.

[15] R. E. Collin and F. J. Zucker, Eds., *Antenna Theory.* New York: McGraw-Hill, 1969.

[16] R. Pregla, "New approach for the analysis of cylindrical antennas by the method of lines," *Electron. Lett.*, vol. 30, no. 8, pp. 614–615, 1994.

[17] Z. Shen and R. H. MacPhie, "Modeling of a monopole partially buried in a grounded dielectric substrate by the modal expansion method," *IEEE Trans. Antennas. Propagat.*, vol. 44, pp. 1535–1536, Nov. 1996.

[18] ——, "Rigorous evaluation of the input impedance of a sleeve monopole by modal-expansion method," *IEEE Trans. Antennas. Propagat.*, vol. 44, pp. 1584–1591, Dec. 1996.

[19] C. L. Chi and N. G. Alexopoulos, "Radiation by a probe through a substrate," *IEEE Trans. Antennas Propagat.*, vol. 34, pp. 1080–1091, Sept. 1986.

[20] S. Pinhas, S. Shtrikman, and D. Treves, "Moment-method solution of the center-fed microstrip disk antenna invoking feed and edge current singularities," *IEEE Trans. Antennas Propagat.*, vol. 37, pp. 1516–1522, Dec. 1989.

Reinhold Pregla (M'76–SM'83) received the Dipl.-Ing. (electrical engineering) and the Dr.-Ing. degrees from the Technical University Braunschweig, West Germany, in 1963 and 1966, respectively.

From 1966 to 1969, he was a Research Assistant in the Department of Electrical Engineering of the Technical University Braunschweig (Institut für Hochfrequenztechnik), where he was engaged in investigations of microwave filters. After the Habilitation, he was a Lecturer in high frequencies at the Technical University Braunschweig. Since 1973 he has held the position of Professor at the Ruhr University, Bochum, Germany, and since 1975 he has held the position of Full Professor in electrical engineering at the Fern Universität (a university for distance study) in Hagen, Germany. His fields of investigation include microwave and millimeter-wave integrated circuits, field theory, antennas, and integrated optics and photonics.